J. Fluid Mech. (2006), *vol.* 567, *pp.* 157–184. © 2006 Cambridge University Press
doi:10.1017/S0022112006002345 Printed in the United Kingdom

A cyclic model for particle motion in the pulmonary acinus

By S. HABER[1] AND A. TSUDA[2]

[1]Department of Mechanical Engineering, Technion, Haifa 32000, Israel
[2]Physiology Program, Harvard School of Public Health, Boston, MA 02115, USA
mersh01@tx.technion.ac.il

(Received 2 September 2004 and in revised form 26 April 2006)

A simplified model for the pulmonary alveolus that imitates the rhythmical expansion of the alveolus and the periodic shear flow in the adjacent airway is explored. The model consists of two eccentric cylinders and incompressible fluid that occupies the gap between them. The two cylinders undergo a simultaneous rhythmical expansion and contraction (mimicking the alveolus expansion) while the inner cylinder performs a periodic rotation about its axis (inducing shear flow mimicking airway ductal flow). An analytical solution is obtained for the creeping flow induced by the simultaneously expanding cylinders. It is shown that above a certain critical value of rotation to expansion velocity ratio, the flow exhibits characteristic features such as a saddle point and closed streamlines about a centre, similar to those existing inside a single alveolus during inhalation and exhalation. Poincaré maps of the trajectories of fluid particles demonstrate that, under various flow conditions, chaotic trajectories may exist, provided that expansion and rotation are slightly out of phase. This is similar to normal breathing conditions where the periodic expansion of the alveolus and the tidal flow (i.e. shear flow above the mouth of the alveolus) may be slightly out of phase. A novel definition of overall convective mixing efficiency is also suggested that inherently discounts reversible processes that do not contribute to mixing. It is demonstrated that two different convective mechanisms, related to the irreversibility of exhalation and inhalation and the onset of chaos, govern mixing efficiency in lung alveoli.

1. Introduction

Investigating the fate of micron and sub-micron particles that may reach the lung acinus (the alveolated part of the lung) is of paramount importance in cases concerning environmental exposure to hazardous aerosols, drug delivery, dosing and gene therapy. The complex structure of the lung that consists of about 16 million duct segments and 300–400 million alveoli (Weibel 1963, 1986) makes it currently impossible to obtain a faithful numerical solution for the lung flow during breathing, a pre-requisite to predicting particles' trajectories and their deposition sites. The flow field that exists inside the acinus is determined by its geometrical configuration and the underlying breathing conditions. The acinus can be viewed as a binary tree of alveolated airways that begins at about the 16th bifurcation and ends normally at the 22nd–23rd generation. The central channels open into multiple sacs (the alveoli), a few hundred microns in diameter. During breathing, the channels and alveoli expand and contract rhythmically and air enters and exits the lung periodically, with a possible time lag between alveoli expansion and central channel flow (Miki *et al.* 1993).

Acinar flow was first studied in a rigid-walled geometric model. A steady low-Reynolds-number flow was numerically solved for an axisymmetric alveolated duct model, which contains a central thoroughfare channel surrounded by numerous doughnut-shaped alveoli (Federspiel & Fredberg 1988; Tsuda, Butler & Fredberg 1994*a*, *b*). Since then, several models with different alveolar shapes have been created and the steady acinar flow has been studied both numerically and experimentally (Tsuda *et al.* 1991; Darquenne & Paiva 1996; Darquenne 2001; Karl, Henry & Tsuda 2004). Tsuda, Henry & Butler (1995) initiated the study on the effects of acinar wall motion associated with tidal breathing on acinar flow by rhythmically expanding and contracting the axisymmetric model in a self-similar fashion. They found that the flow can exhibit chaotic behaviour when the creeping oscillatory recirculation flow inside the expanding/contracting alveolus was perturbed to include non-zero Reynolds number effects. In a more recent model, we employed a fully three-dimensional model (Haber *et al.* 2000) where the unit system of alveolus and neighbouring duct consisted of a single periodically expanding and contracting hemi-spherical alveolus attached to an expanding flat plate. The alveolus was also subjected to periodic, out-of-phase shear flow at the mouth of the alveolus. As a first approximation, inertial effects were ignored, and the creeping flow limit was assumed. The governing linear Stokes equations made it possible to superimpose the effects of alveolar expansion/contraction and of ductal air intake.

These previous theoretical analyses, however, relied heavily on numerical solutions of the flow fields. For instance, in Tsuda *et al.* (1995) and Henry, Butler & Tsuda (2002) a fully numerical approach was employed. In Haber *et al.* (2000) the alveolar expansion problem possesses an analytical solution (given by a converging infinite series) but the shear flow problem was solved using a numerical approach (Pozrikidis 1994). These analyses may be limited, in particular when mixing properties of the system are sought. The stream function needs to be differentiated twice to obtain the local strain rates, an operation that could lead to large numerical errors. The complexity of the previous models, a combination of time-dependent geometrical configuration and kinematical conditions, led us to believe that further progress can be made if a fully analytical solution can be obtained for a simpler model that possesses dynamical features similar to those obtained in Tsuda *et al.* (1995) and Haber *et al.* (2000).

The most basic feature of alveolar flow is the presence of a recirculation flow inside a dead-end side pocket (i.e. alveolus) driven by a shear flow passing over the mouth of the alveolus (Federspiel & Fredberg 1988; Tsuda *et al.* 1994*a*, *b*, 1995, 2002; Darquenne & Pavia 1996; Darquenne 2001; Haber *et al.* 2000; Haber & Tsuda 2003; Henry *et al.* 2002; Tippe & Tsuda 2000). Inspired by the pioneering work of Aref (1984), we revealed that this basic feature is markedly similar to that of the well-known journal-bearing flow, namely, a recirculation flow in the space between two cylinders, driven by the eccentric rotating of the inner cylinder. In figure 1, the alveolar flow and the journal-bearing flow are shown side by side. Figure 1(*a*) illustrates a streamline map of the three-dimensional non-expanding alveolus (Pozrikidis 1994). Figure 1(*b*) is a two-dimensional projection of its central plane. Figure 1(*c*) depicts the streamline map of the journal-bearing flow for rotating cylinders (Ballal & Rivlin 1976). Both maps possess a centre and two stagnation points connected by a separating streamline (the broken line shown in (*b*) and (*c*)). The wall of the rotating inner cylinder (figure 1*c*) can be perceived as an undisturbed streamline of the shear flow that exists in an airway adjacent to the alveolus (the straight line shown in the figure 1*b*). This flow similarity suggests that the larger space between the dividing streamline and the wall of the outer cylinder can be considered as the alveolus while the space between the

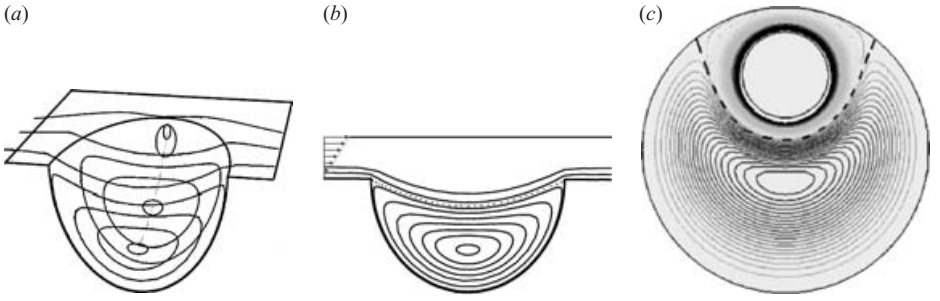

FIGURE 1. (*a*, *b*) Streamlines generated inside a three-dimensional alveolus and at its mid-plane, from Pozrikidis (1994) (reprinted with permission from C. Pozrikidis, figure 4b published in *Phys. Fluids* vol. 6, pp. 68–79, Copyright 1994 American Institute of Physics). (*c*) Streamlines generated by a rotating inner cylinder similar to Ballal & Rivlin 1976). The broken line in (*b*, *c*) illustrates a streamline dividing the space between two non-mixing regions: the alveolus and the adjacent airway regions.

dividing streamline and the wall of the inner cylinder represents that part of the acinar duct where a shear flow is passing over the mouth of the alveolus.

Including the effect of alveolar expansion, Tsuda *et al.* (1995) and Haber *et al.* (2000) showed that the flow field deviated from the pattern shown in figure 1(*b*) and revealed rich patterns; e.g. under typical conditions the streamline map possessed two equilibrium points: a saddle and a centre surrounded by a homoclinic orbit. Such features in dynamical systems are known to be intimately related to instability under small perturbations that may lead to chaos. Haber *et al.* (2000) indicated that chaotic trajectories may exist under the effect of small velocity perturbations generated by alveolar expansion juxtaposed with a phase lag between the periodical shear- and the expansion-induced flows observed in real lungs. Many other, somewhat similar, flow systems revealing chaotic behaviour have been investigated in the past (e.g. Aref 1984; Ottino *et al.* 1988). For instance, Aref (1984), and Aref & Balachandar (1986) showed that chaotic trajectories may exist in the Stokesian flow bounded between two eccentric cylinders performing a 'blinking' periodic rotation. Hydon (1994*a*, *b*) addressed the fully developed quasi-steady oscillatory flow in a curved pipe where the velocity components at the transverse plane can be derived from a stream function. The effect of a small perturbation due to unsteady inertia (small Womersley numbers) was explored. It was shown that the non-perturbed flow in the two-dimensional space of the cross-section plane can be represented by an autonomous integrable one-degree-of-freedom Hamiltonian system (with a proper transformation of the time variable). Trajectories of a tracer moving in the perturbed near-integrable dynamical system may form 'islands', in accordance with KAM theory, and chaotic regions surrounding those islands. Solomon, Weeks & Swinney (1994) investigated experimentally the two-dimensional flow in a rotating annulus, again analysing the effects of inertia on the flow, revealing KAM tori and large regions with chaotic trajectories.

The objective of this study is to suggest a simplified model of the time-dependent rhythmically expanding alveolar flow, for which an exact analytical solution exists. Such a solution would enable us to seek: the dependence of the main dynamical properties upon the geometrical and kinematical parameters of the system; the fluid trajectories and the possible onset of chaos; and the evaluation of mixing and its relation to the chaotic behaviour of particle trajectories.

The foregoing goals were achieved in the following three sections. Section 2 describes the geometrical and kinematical properties of the model and analyses the streamline

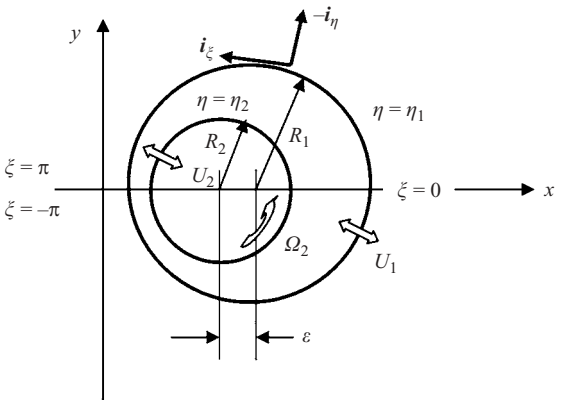

FIGURE 2. Configuration of the two eccentric cylinders and the corresponding values of the bi-polar coordinates defining their moving walls. Fluid occupies the gap between the cylinders.

maps. Section 2.1 includes a short recapitulation of the known solution for two rotating eccentric cylinders. Section 2.2 addresses the case of two eccentric radially expanding cylinders, bounding an incompressible fluid and a novel exact analytical solution is obtained. In § 2.3 the combined flow properties are described. Section 3 is devoted to the dynamical behaviour of fluid particles and its effect on mixing. In § 3.1 fluid particle trajectories are computed and Poincaré maps are provided for different breathing time protocols that illustrate the possible chaotic nature of the flow. In § 3.2, a global approach is discussed by which mixing efficiency dependence on the flow parameters can be estimated and chaos-related behaviour of mixing efficiency is revealed. In § 4 we summarize the main results and conclusions and the limitations of the model.

2. A cyclic flow model of the acinus

Consider two non-concentric cylinders of radii R_1 and $R_2 (R_2 < R_1)$ and eccentricity ε (see figure 2). An incompressible fluid of density ρ and viscosity μ occupies the gap between the cylinders. The outer cylinder performs a periodic radial expansion motion $U_1(t/T)$ with respect to its centre. The inner cylinder rotates with a time-dependent periodic angular velocity $\Omega_2(t/T, \delta)$ and performs a radial expansion motion $U_2(t/T)$, with respect to its centre, so that the volume between the cylinders remains fixed, thus satisfying the condition that the flow is incompressible. Here, T denotes the breathing period and δ stands for the phase-lag angle between the two periodic motions. Notice that Ω_2 and U_1 are associated with the forced flow intake during breathing, and the boundary condition at the alveolus wall during lung expansion, respectively.

Assuming that the Reynolds numbers $|\Omega_2 R_2^2 \rho/\mu|$ and $|U_1 R_1 \rho/\mu|$ are much smaller than unity (conditions satisfied by the flow fields in the acinar region), the equations governing the flow are the quasi-steady Stokes equations,

$$\nabla \cdot \boldsymbol{v} = 0, \tag{1a}$$

$$\mu \nabla^2 \boldsymbol{v} = \nabla p, \tag{1b}$$

where $\boldsymbol{v}$ and p are the fluid velocity and pressure fields, respectively.

The velocity field is subjected to the following boundary conditions:

$$\boldsymbol{v} \cdot \boldsymbol{i}_\eta = -U_1 \quad \text{and} \quad \boldsymbol{v} \cdot \boldsymbol{i}_\xi = 0 \qquad \text{at the wall of cylinder 1 } (\eta = \eta_1), \tag{2a}$$

$$\boldsymbol{v} \cdot \boldsymbol{i}_\eta = -U_2 \quad \text{and} \quad \boldsymbol{v} \cdot \boldsymbol{i}_\xi = \Omega_2 R_2 \qquad \text{at the wall of cylinder 2 } (\eta = \eta_2). \tag{2b}$$

Here, the natural bi-polar coordinate system (η, ξ) is used (Happel & Brenner 1964, see also figure 2) according to the following transformations:

$$x = c\frac{\sinh\eta}{\cosh\eta - \cos\xi} \quad \text{and} \quad y = c\frac{\sin\xi}{\cosh\eta - \cos\xi}, \tag{3}$$

where $\boldsymbol{i}_\eta$ and $\boldsymbol{i}_\xi$ are the respective radial and tangential unit vectors and η_1 and η_2 determine the boundaries of cylinders 1 and 2, easily evaluated from the following identities:

$$\sinh\eta_1 = c/R_1, \quad \sinh\eta_2 = c/R_2, \tag{4a}$$

where

$$c = \left[\left(R_1^2 + R_2^2 - \varepsilon^2\right)^2 - 4R_1^2R_2^2\right]^{1/2}/2\varepsilon. \tag{4b}$$

Notice that R_1 and R_2 are time dependent as are c, η_1 and η_2. However, this does not introduce complications since the Stokes equations are quasi-steady and only the instantaneous configuration affects the flow. Consequently, the solution of equations (1) and (2) can be obtained by addressing two separate cases: (*a*) the flow generated by two rotating non-expanding cylinders and (*b*) the flow induced by expanding non-rotating cylinders. Superposition of these two cases would result in the solution of (1) and (2) sought.

2.1. *The flow generated by two rotating non-expanding eccentric cylinders*

The solution of (1) and (2) for $U_1 = U_2 = 0$ is well known (e.g. Ballal & Rivlin 1976) for the more general case of two cylinders rotating with angular velocities Ω_1 and Ω_2. A brief recapitulation of the solution is presented here. The solution for the stream function employing the bi-polar coordinate system is

$$\Psi^{ROT} \equiv \Omega_2 R_2 c \psi^{ROT} = \Omega_2 R_2 c[F_0(\eta) + F_1(\eta)\cos\xi]/(\cosh\eta - \cos\xi) \tag{5a}$$

where

$$F_0(\eta) = (A_0 + C_0\eta)\sinh\eta + (B_0 + D_0\eta)\cosh\eta, \tag{5b}$$

$$F_1(\eta) = A_1\sinh(2\eta) + B_1\cosh(2\eta) + C_1 + D_1\eta, \tag{5c}$$

and the coefficients $A_0, B_0, \ldots, D_1$ are functions of η_1 and η_2 (see Appendix A).

The velocity components v_η and v_ξ are easily derived from the stream function,

$$v_\eta = -\frac{(\cosh\eta - \cos\xi)}{c}\frac{\partial\Psi^{ROT}}{\partial\xi}, \tag{6a}$$

$$v_\xi = \frac{(\cosh\eta - \cos\xi)}{c}\frac{\partial\Psi^{ROT}}{\partial\eta}. \tag{6b}$$

Figure 1(*c*) illustrates that, for large eccentricities and $\Omega_1 = 0$, the flow in the wide gap between the cylinders contains two distinct regions (defined by a separating streamline, shown by the broken line). The wide gap region near the outer cylinder (below the broken line) possesses characteristic flow structures that resemble those shown in Haber *et al.* (2000) for recirculation flow induced inside a rigid alveolus by shear flow in the adjacent airway. The flow in the narrow gap region near the inner cylinder (above the broken line) resembles the fast shear flow in an airway adjacent to the mouth of the alveolus.

For the sake of completeness, we also provide the pressure field that exists in this case:

$$P^{ROT} = P_0 + \frac{2\mu\Omega_2 R_2}{c}\{[A_1\cosh\eta + (2B_1 - C_0)\sinh\eta]\sin\xi - [A_1\cosh(2\eta) + B_1\sinh(2\eta)]\sin(2\xi)\}. \tag{6c}$$

2.2. *The flow field generated by expanding non-rotating eccentric cylinders*

An analytical solution for the incompressible creeping flow field that is generated by two expanding non-concentric cylinders has not been obtained in the past, to the best of our knowledge. In previous papers, the common approach was to rewrite equations (1*a*, *b*) in bi-polar coordinates to yield the following governing equations for the stream function:

$$\Psi^{EXP} = c(\cosh\eta - \cos\xi)^{-1}\Phi, \tag{7a}$$

$$\frac{\partial^4\Phi}{\partial\xi^4} + 2\frac{\partial^4\Phi}{\partial\xi^2\partial\eta^2} + \frac{\partial^4\Phi}{\partial\eta^4} + 2\frac{\partial^2\Phi}{\partial\xi^2} - \frac{\partial^2\Phi}{\partial\eta^2} + \Phi = 0. \tag{7b}$$

To solve (7*b*), a separation of variables technique is normally applied that yields the following general infinite series:

$$\begin{aligned}
\Phi = {} & A_0\sinh\eta + B_0\cosh\eta + C_0\,\eta\sinh\eta + D_0\eta\cosh\eta \\
& + [A_1\sinh(2\eta) + B_1\cosh(2\eta) + C_1 + D_1\eta]\cos\xi \\
& + \sum_{2}^{\infty}[A_n\sinh(n+1)\eta + B_n\cosh(n+1)\eta + C_n\sinh(n-1)\eta + D_n\cosh(n-1)\eta]\cos(n\xi) \\
& + [\widetilde{A}_0\sinh\eta + \widetilde{B}_0\cosh\eta + \widetilde{C}_0\eta\sinh\eta + \widetilde{D}_0\eta\cosh\eta]\xi \\
& + [\widetilde{A}_1\sinh(2\eta) + \widetilde{B}_1\cosh(2\eta) + \widetilde{C}_1 + \widetilde{D}_1\eta]\sin\xi \\
& + \sum_{2}^{\infty}[\widetilde{A}_n\sinh(n+1)\eta + \widetilde{B}_n\cosh(n+1)\eta + \widetilde{C}_n\sinh(n-1)\eta + \widetilde{D}_n\cosh(n-1)\eta]\sin(n\xi) \\
& + E_0\xi\sin\xi + \widetilde{E}_0\xi\cos\xi
\end{aligned} \tag{8}$$

where $A_0, B_0, \ldots, E_0$ are unknown constants to be determined.

Notice, that the solution (5) for rotating non-expanding cylinders is a truncated expression that contains only the first two lines of expression (8). The solution is symmetric with respect to $\xi = 0$ and cyclic with period 2π in ξ. Lines 4 to 6 contain antisymmetric terms that may be required in case of expanding cylinders. Lines 4 and 7 are normally omitted since they present non-single-valued terms at, for instance, $\xi = -\pi$ and $\xi = \pi$ (the same physical point) and violate the periodicity condition that is commonly required. In our case, however, we desire that the stream function be non-single-valued; a simple explanation of this is as follows. Since the stream function represents the cumulative flow rate from a reference value (say at $\xi = -\pi$) it must increase monotonically as ξ varies from $\xi = -\pi$ to $\xi = \pi$. Consequently, its values at $\xi = -\pi$ and $\xi = \pi$ must differ by the total flow rate (per unit cylinder length) $2\pi R_1 U_1$ that is induced by the expanding cylinders. (Had the cylinders been axisymmetric, the well-known solution for the stream function would have been $\psi = R_1 U_1 \theta$ where θ is the polar angle. Thus, ψ is obviously not single-valued, but assumes different values for $\theta = \pi$ and $\theta = -\pi$, the same physical point.)

Employing (6) and boundary conditions (2), rewritten in bi-polar coordinates for non-rotating cylinders, yields

$$\left.\frac{\partial\Psi^{EXP}}{\partial\xi}\right|_{\eta=\eta_i} = \frac{\partial}{\partial\xi}[\Psi^{EXP}]_{\eta=\eta_i} = \frac{U_i c}{\cosh\eta_i - \cos\xi} \quad \text{at} \quad \eta = \eta_i \ \ (i = 1, 2), \tag{9a}$$

$$\left.\frac{\partial\Psi^{EXP}}{\partial\eta}\right|_{\eta=\eta_i} = 0 \qquad \text{at} \quad \eta = \eta_i \ \ (i = 1, 2). \tag{9b}$$

Integrating (9*a*) with respect to ξ (Gradshtyn & Ryzhik 1984) results in a useful expression for Ψ^{EXP}at the boundaries,

$$[\Psi^{EXP}]_{\eta=\eta_i} = \frac{2U_i c}{\sinh \eta_i} \arctan\left(\frac{\tan(\xi/2)}{\tanh(\eta_i/2)}\right) \quad \text{at} \quad \eta = \eta_i \ \ (i = 1, 2). \tag{10}$$

Notice that

$$\Psi^{EXP}\big|_{\xi=\pi} - \Psi^{EXP}\big|_{\xi=-\pi} = \pi c(U_1/\sinh \eta_1 + U_2/\sinh \eta_2) = \pi(U_1 R_1 + U_2 R_2) = 2\pi U_1 R_1$$

as discussed previously. Thus, from (10) and (7*a*) the corresponding boundary conditions for Φ are

$$[\Phi]_{\eta=\eta_i} = 2U_i \frac{(\cosh \eta_i - \cos \xi)}{\sinh \eta_i} \arctan\left(\frac{\tan(\xi/2)}{\tanh(\eta_i/2)}\right) \qquad (i = 1, 2). \tag{11a}$$

Similarly, employing the above result and (7*a*), the associated boundary condition for Φ, replacing (9*b*), is

$$\left.\frac{\partial \Phi}{\partial \eta}\right|_{\eta=\eta_i} = 2U_i \arctan\left(\frac{\tan(\xi/2)}{\tanh(\eta_i/2)}\right) \qquad (i = 1, 2). \tag{11b}$$

If one attempts to utilize the general representation (8) and the foregoing boundary conditions to determine the unknown coefficients, an infinite series solution for Φ (all terms with a tilde) will be required.

A more ingenious approach is to express Ψ^{EXP} as follows (a clue to this choice is given by boundary condition (10)):

$$\Psi^{EXP} \equiv Uc\psi^{EXP} = Uc\left\{2\arctan\left(\frac{\tan(\xi/2)}{\tan(\eta/2)}\right) + \frac{\widetilde{\Phi}}{\cosh \eta - \cos \xi}\right\} \tag{12}$$

within the domain $\eta_1 < \eta < \eta_2$, $-\pi < \xi < \pi$ where the 'mutual' velocity

$$U = U_i/\sinh \eta_i \qquad (i = 1, 2) \tag{13}$$

is independent of i, since the incompressibility condition requires that $2\pi R_1 U_1 = 2\pi R_2 U_2$ or from (4*a*) that $U_1/\sinh \eta_1 = U_2/\sinh \eta_2$.

The yet undetermined function $\widetilde{\Phi}$ satisfies equation (7*b*) and possesses periodic antisymmetric terms only (generally, lines 4 and 5 in (8)). Also notice that the first term in (12) is a valid solution of the Stokes equations. This can easily be verified by direct substitution into the bi-harmonic partial differential equation governing the stream function in bi-polar coordinates,

$$\left(\frac{\partial^2}{\partial \xi^2} + \frac{\partial^2}{\partial \eta^2}\right)\left[(\cosh \eta - \cos \xi)^2 \left(\frac{\partial^2}{\partial \xi^2} + \frac{\partial^2}{\partial \eta^2}\right)\right]\Psi = 0.$$

Substitution of (12) into (10) and (9*b*) results in the associated very simple boundary conditions for $\widetilde{\Phi}$

$$[\widetilde{\Phi}]_{\eta=\eta_i} = 0 \qquad (i = 1, 2), \tag{14a}$$

$$\left[\frac{\partial \widetilde{\Phi}}{\partial \eta}\right]_{\eta=\eta_i} = \sin \xi \qquad (i = 1, 2). \tag{14b}$$

Obviously, a solution for $\widetilde{\Phi}$ is now trivial and the only non-vanishing coefficients to be determined are $\widetilde{A_1}, \widetilde{B_1}, \widetilde{C_1}$ and $\widetilde{D_1}$ in (8). These are easily derivable by direct

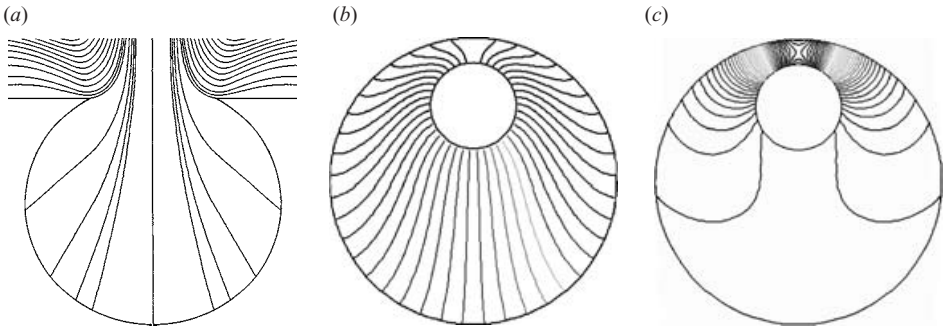

FIGURE 3. (*a*) The streamlines in an expanding alveolus obtained by Haber *et al.* (2000). (*b*) Streamlines for expanding non-rotating cylinders. (*c*) Pressure isobars for expanding cylinders ($R_2/R_1 = 0.3$, $\varepsilon/R_1 = 0.525$).

substitution of (8) into (14) to yield

$$\widetilde{\Phi} = \frac{\sin\xi}{\Delta_1}[-(\eta_2-\eta_1)\sinh(\eta_1+\eta_2-2\eta)+(\eta_1+\eta_2-2\eta)\sinh(\eta_2-\eta_1)] \quad (15a)$$

where

$$\Delta_1 = 2[(\eta_2-\eta_1)\cosh(\eta_2-\eta_1)-\sinh(\eta_2-\eta_1)]. \quad (15b)$$

Consequently, an analytical expression was obtained that contains a finite number of terms for the stream function (a combination of (12) and (15)) that governs the flow field generated by two expanding non-rotating eccentric cylinders. For the sake of completeness, the pressure field was also obtained,

$$p^{EXP} = \frac{2\mu U}{c\Delta_1}\{-2[(\eta_2-\eta_1)\cosh(\eta_1+\eta_2-\eta)+\sinh(\eta_2-\eta_1)\cosh\eta]\cos\xi + (\eta_2-\eta_1)\cosh(\eta_2+\eta_1-2\eta)\cos(2\xi)\}. \quad (16)$$

Figure 3(*a*) illustrates the streamlines in an expanding alveolus obtained by Haber *et al.* (2000). Figure 3(*b*) illustrates the typical behaviour of the stream function, a monotonic increase in value from $\xi = -\pi$ to π and streamlines terminating perpendicularly at the cylindrical walls. Figure 3(*c*) illustrates pressure isobars for the same case. This deviates noticeably from the known uniform pressure field that exists in the gap between concentric radially expanding cylinders.

2.3. *The combined flow field for rotating and expanding cylinders*

The combined quasi-steady solution for rotating and expanding cylinders

$$\Psi = c(U\psi^{EXP} + \Omega_2 R_2 \psi^{ROT}) \quad (17)$$

depends linearly on the angular velocity Ω_2 and expansion velocity U, that may be defined by quite arbitrary time-dependent functions. Their magnitudes and time derivatives must, however, comply with the conditions imposed on quasi-steady creeping flows, namely, that the corresponding Reynolds and Womersley numbers are smaller than unity. Also notice that since ψ^{EXP} is not a single-valued function that possesses a finite jump between $\xi = \pi$ and $\xi = -\pi$, the combined stream function Ψ in (17) is also an aperiodic non-single-valued function.

At a given time, the streamline map depends on the instantaneous value of the velocity ratio

$$\kappa = \Omega_2 R_2 / U. \quad (18)$$

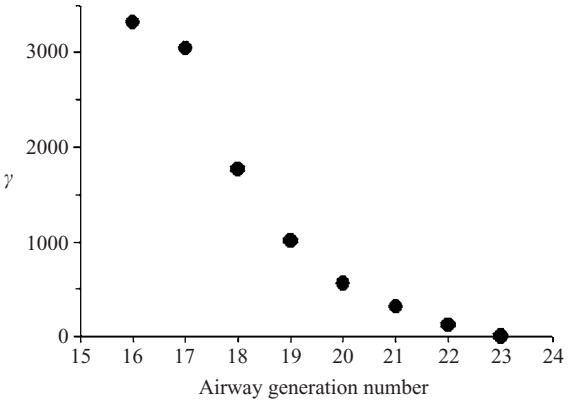

FIGURE 4. The dependence of γ on the airway generation along the acinar tree. γ also represents the ratio between the flow shear rate at the wall of the acinar duct to the strain rate of the alveolus.

In Haber & Tsuda (2003) we similarly defined the shear parameter $\gamma = GR/\dot{R}$ that was the ratio between the flow strain rate approaching the alveolus mouth and the expansion rate per alveolus radius. Since γ is directly related to airway generation (figure 4) it is relevant to obtain a similar relation for the current model. Thus, if G scales with the strain rate at the narrow gap between the cylinders $\Omega_2 R_2/(R_1 - R_2 - \varepsilon)$, the alveolus radius scales with R_1 and $\dot{R}$ with U_1, a simple linear relation exists between κ and γ that depends solely on the geometrical arrangement of the cylinders,

$$\gamma = \kappa \frac{R_1^2}{c(R_1 - R_2 - \varepsilon)}. \tag{19}$$

Thus, high values of κ correspond to high values of γ, etc. and, consequently, for a fixed geometrical configuration, various κ values represent alveoli at different acinar airway tree generations. Figure 5(a, b) depicts the streamline maps inside an expanding cavity of our previous three-dimensional alveolar model and our current two-dimensional model. Figure 5(a) illustrates that at an intermediate value of $\gamma = 400$, recirculation flow with a saddle point and a centre already occur, while for a smaller value of $\gamma = 200$ (figure 5b) neither recirculation flows nor centres nor saddle points are obtained. Note that the former case occurs at alveoli up to the 20th airway generation (see figure 4), where the flow is a balance between rotating flow driven by the airway ductal shear flow and the flow induced by the alveolar wall expansion. The latter case corresponds to alveolar flows deep in the acinus where the flow is mainly determined by the expansion motion of the alveolus boundary.

We shall, henceforth, assume that the external cylinder undergoes periodic expansion and contraction,

$$R_1 = R_0[1 - \beta \cos(2\pi t/T)], \tag{20}$$

with small values of $\beta < 0.1$ that correspond to a range of realistic volumetric expansions of a lung alveolus. From (20), the wall velocity of the outer cylinder '1' is $U_1 = (2\pi R_0 \beta/T)\sin(2\pi t/T)$ and correspondingly, the 'mutual' velocity U is

$$U = (2\pi R_0 \beta R_1/Tc)\sin(2\pi t/T). \tag{21}$$

In addition, following Aref & Balachandar (1986), we applied different schemes for time modulation of the angular velocity Ω_2 (figure 6). The first periodic time protocol (A), shown schematically (figure 6a), employs a simple step function in which the

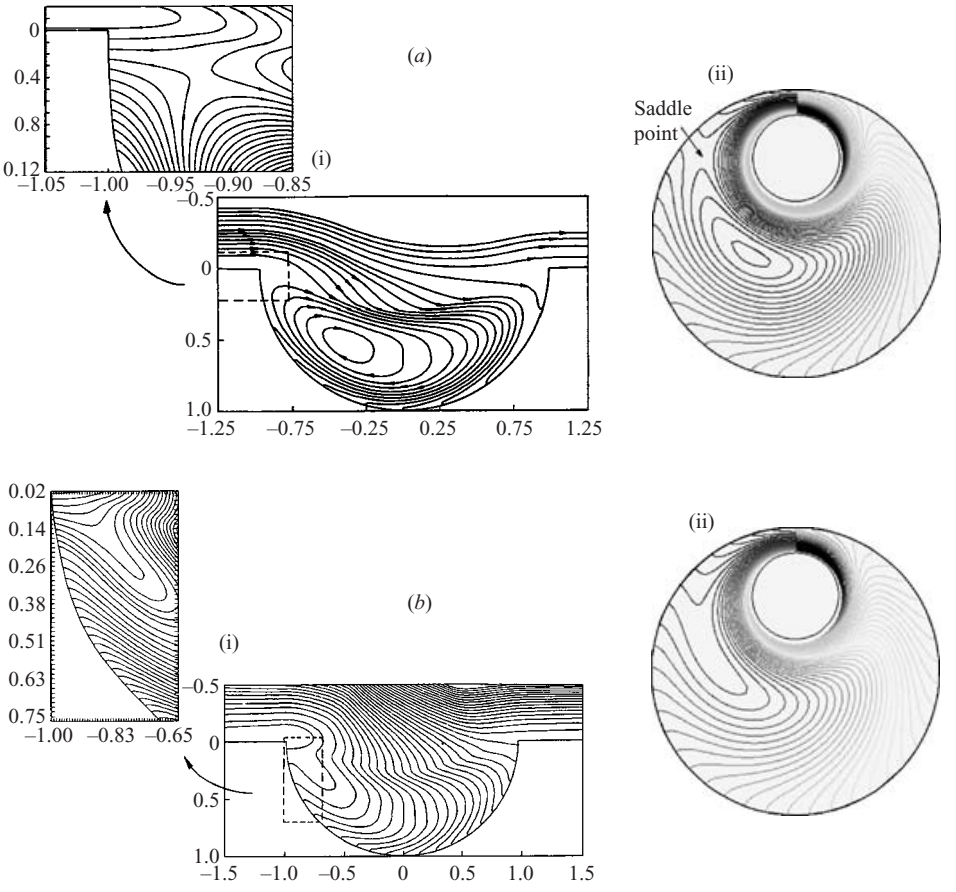

FIGURE 5. (i) Streamlines at the three-dimensional model midsection, from Haber *et al.* (2000). (ii) Streamlines for an expanding system and a rotating inner cylinder. $\bar{R}_2/\bar{R}_1 = 0.3$, $\varepsilon/\bar{R}_1 = 0.525$, $\beta = 0.02$. (*a*) A saddle point can be observed for $\Omega T = 100$. (*b*) No saddle point is observed for $\Omega T = 60$.

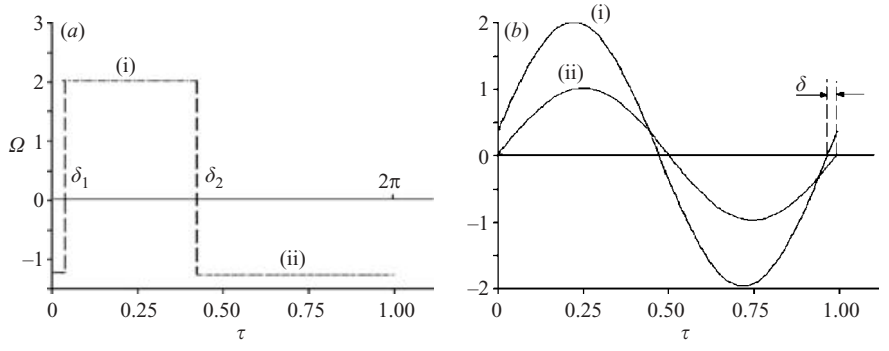

FIGURE 6. (*a*) Time protocol A. Angular velocity variation during a single breathing period with unequal inhalation ($\delta_1 < 2\pi\tau < \delta_2$) and exhalation ($0 < 2\pi\tau < \delta_1$ and $\delta_2 < 2\pi\tau < 2\pi$) durations. The values of Ω during exhalation (Ω_B) and inhalation (Ω_A) are correlated $\Omega_B = \Omega_A(\delta_2 - \delta_1)/(2\pi - \delta_2 + \delta_1)$. (*b*) Time protocol B. The sinusoidal time protocol where $\tau = t/T$ denotes the dimensionless time, (i) pertains to the time variation of the angular velocity of the inner cylinder and (ii) the rate of expansion of the outer cylinder.

inhalation (rotation in one direction) and exhalation (rotation in the opposite direction) times are unequal. For given inhalation and exhalation durations, the associated amplitudes are correlated, subject to the condition that a zero net fluid volume passes over the gap between the cylinders after a complete breathing period T. Here, again, we assumed a phase lag between the initiation of the shear- and expansion-induced flows.

The second time protocol (B) describes schematically a sinusoidal variation with a small phase lag angle δ (less than $\pi/18 = 10^\circ$) between rotation- and expansion-induced flows,

$$\Omega_2 = \Omega \sin(2\pi t/T + \delta), \tag{22}$$

as observed by Miki *et al.* (1993). Notice, that for $\delta = 0$ the value of γ in (19) remains bounded for all times and can be approximated by the time-mean values of R_1 and R_2, $\overline{R}_1 = R_0$, $\overline{R}_2 \approx \sqrt{R_0^2 - S/\pi}$, the latter expression including a small error of order β where S is the time-independent volume per unit length bounded between the two cylinders.

Consequently, the approximate value of γ in (19) (to a small error of order 1),

$$\gamma \approx \frac{\Omega T}{2\pi\beta} \frac{\overline{R}_2}{\overline{R}_1 - \overline{R}_2 - \varepsilon}, \tag{23}$$

can be applied in a manner similar to that used by Haber & Tsuda (2003) to evaluate the airway generation number. The inaccuracy introduced in (23) of $O(1)$ is, indeed, small since γ values are generally of $O(10^2$–$10^3)$.

Thus, the flow field generated by a rotating inner cylinder and expanding cylinders is determined by the rotational time protocols and the three parameters β, γ, and δ of which γ (the ratio between shear and expansion rates) is directly related to the airway generation number. The ratio between the inhalation and exhalation durations (as defined in time protocol A), is an additional parameter, not investigated in Haber & Tsuda (2003). This ratio is not necessarily equal to one, as may occur under real breathing conditions.

A final remark relates to the choice of the geometrical configuration and the kinematical parameters that we employed for this model. The value of β defines the alveolar expansion so that it may range between 0.02 and 0.05, representing a three-dimensional volumetric expansion of about 12% to 30%, common to human alveoli (e.g. Fredberg 2000). Time was scaled by T, lengths by R_0, velocities by R_0/T and angular velocities by $1/T$. Thus, we were still free to choose the dimensionless values of $\overline{R}_2$ and ε. This choice was affected by two requirements: (i) that a streamline map similar to that shown in figure 3 is obtained (for small eccentricities a separating streamline is not obtained) and (ii) that a saddle point (see figure 5) appears at a γ value obtained in our previous paper (Haber *et al.* 2000). These requirements were not difficult to satisfy and representative values of either ($\overline{R}_2 = 0.3$, $\varepsilon = 0.525$, $\beta = 0.02$) or ($\overline{R}_2 = 0.5$, $\varepsilon = 0.4$, $\beta = 0.05$) were employed for a γ range between zero and 4000. Employing (23) we obtain that for the former case $\gamma = 85.7\,\Omega T$ and for the latter $\gamma = 100\,\Omega T$.

3. Results and discussion

3.1. *Particle trajectories and Poincaré maps*

The trajectory of a massless particle moving in the flow generated by the expanding and rotating cylinders is determined by the following equations:

$$v_x = \frac{\mathrm{d}x}{\mathrm{d}t} = \frac{\partial \Psi}{\partial y}, \qquad v_y = \frac{\mathrm{d}y}{\mathrm{d}t} = -\frac{\partial \Psi}{\partial x},$$

where Ψ is a function of x, y and t, or equivalently, ξ, η and t. This form suggests that the system is governed by a time-dependent Hamiltonian H where $H \equiv \Psi$ and the pair x and y represents a single degree of freedom (Lichtenberg & Lieberman 1992). With that interpretation, the KAM theorem may be employed to explain how a sufficiently small perturbation parameter (in our case the phase angle δ) affects only slightly some of the closed non-perturbed streamlines to form KAM tori. In addition the Poincaré–Birkhoff theorem also suggests that some of the closed streamlines will break up to form stochastic trajectories bounded by the KAM tori (see also Tabor 1989; Ottino 1989 and Horner *et al.* 2002 that deal with the effect of Reynolds number perturbations in cavity flows).

A more detailed description of how our system can be viewed as the sum of two Hamiltonians one associated with an integrable system and the other with the perturbed one is deferred to Appendix B.

Excluding Brownian motion, gravity and inertia effects, the following equations govern the motion of a fluid particle (in terms of the more natural coordinates ξ, η, see Appendix C):

$$\frac{\mathrm{d}\xi}{\mathrm{d}t} = \frac{(\cosh\eta - \cos\xi)^2}{c^2}\frac{\partial\Psi}{\partial\eta} + \frac{\cosh\eta\sin\xi}{c}\frac{\mathrm{d}c}{\mathrm{d}t}, \tag{24a}$$

$$\frac{\mathrm{d}\eta}{\mathrm{d}t} = -\frac{(\cosh\eta - \cos\xi)^2}{c^2}\frac{\partial\Psi}{\partial\xi} + \frac{\sinh\eta\cos\xi}{c}\frac{\mathrm{d}c}{\mathrm{d}t}, \tag{24b}$$

where Ψ is the combined stream function defined in (17) and

$$\frac{\mathrm{d}c}{\mathrm{d}t} = -\frac{R_1}{c}\frac{\mathrm{d}R_1}{\mathrm{d}t} = -U.$$

A straightforward substitution of (5), (12) and (15) into (24) results in a system of two nonlinear ordinary differential equations where the right-hand side depends explicitly on ξ, η and time,

$$\begin{aligned}\frac{\mathrm{d}\xi}{\mathrm{d}t} = \frac{U}{c}\sin\xi\Bigg\{&-(2\cosh\eta - \cos\xi) - \frac{\sinh\eta}{2\Delta_1}[-(\eta_2-\eta_1)\sinh(\eta_2+\eta_1-2\eta) + (\eta_2+\eta_1-2\eta)\\ &\times \sinh(\eta_2-\eta_1)] + \frac{(\cosh\eta-\cos\xi)}{\Delta_1}[(\eta_2-\eta_1)\cosh(\eta_2+\eta_1-2\eta)\\ &- \sinh(\eta_2-\eta_1)]\Bigg\} + \frac{\Omega_2 R_2}{c}\{A_0(1-\cosh\eta\cos\xi) - B_0\sinh\eta\cos\xi\\ &+ C_0[\eta(1-\cosh\eta\cos\xi) + \sinh\eta(\cosh\eta-\cos\xi)] + D_0[-\eta\sinh\eta\cos\xi\\ &+ \cosh\eta(\cosh\eta-\cos\xi)] + A_1\cos\xi[-\sinh\eta\sinh(2\eta) + 2(\cosh\eta-\cos\xi)\\ &\times\cosh(2\eta)] + B_1\cos\xi[-\sinh\eta\cosh(2\eta) + 2(\cosh\eta-\cos\xi)\sinh(2\eta)]\\ &- C_1\sinh\eta\cos\xi + D_1\cos\xi(-\eta\sinh\eta + \cosh\eta - \cos\xi)\},\end{aligned} \tag{25a}$$

$$\begin{aligned}\frac{\mathrm{d}\eta}{\mathrm{d}t} = \frac{U}{c}\Bigg\{&-\sinh\eta\cosh\eta - \frac{\cos\xi\cosh\eta - 1}{2\Delta_1}[-(\eta_2-\eta_1)\sinh(\eta_2+\eta_1-2\eta)\\ &+ (\eta_2+\eta_1-2\eta)\sinh(\eta_2-\eta_1)]\Bigg\} + \frac{\Omega_2 R_2}{c}\{\sin\xi(A_0\sinh\eta + B_0\cosh\eta\\ &+ C_0\eta\sinh\eta + D_0\eta\cosh\eta) + \sin\xi\cosh\eta[A_1\sinh(2\eta)\\ &+ B_1\cosh(2\eta) + C_1 + D_1\eta\}.\end{aligned} \tag{25b}$$

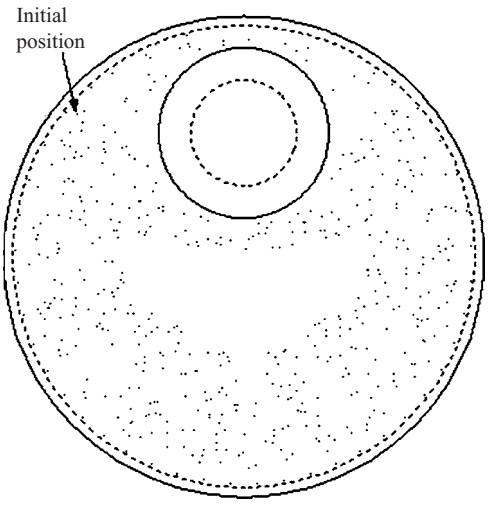

FIGURE 7. Poincaré map for a single particle introduced initially at $(\eta_i, \xi_i) = (0.6, \pi/3)$ and its position sampled after each breathing period during 500 breathing cycles. Chaotic behaviour can be observed. Rotation of inner cylinder is according to protocol A (figure 6) with $\delta_1 = \pi/18$ and $\delta_2 = 5\pi/6$ and $\Omega T = 20$ associated with airway generation 18. The geometrical configuration is defined in figure 5 where the dotted and full circles pertain to the minimum and maximum size of the cylinders at the onset of inhalation and exhalation, respectively.

Here, A_0, B_0, etc. are time-dependent functions (since η_1 and η_2 vary with time) given in Appendix A.

Notice that the dynamic system (25) possesses three dimensions (η, ξ, τ), the minimum required to exhibit chaotic behaviour (Tabor 1989). In past models that have been used to investigate particle trajectories in alveoli, the right-hand-side expressions were either given numerically or consisted of an infinite sum. The right-hand-side analytical expression of system (25), however, can be evaluated efficiently at any desired time and spatial location, thus avoiding sum truncations or interpolations between adjacent grid points. Such high accuracy is greatly desired, in particular if chaotic trajectories are expected.

We also notice that for $\delta = 0$, no phase lag exists between the rotation- and expansion-induced flows and the solution should exhibit a simple periodic motion, as a result of the reversibility of the quasi-stationary Stokes equations of motion. Consequently, this case can conveniently be employed to verify the accuracy of any chosen numerical code. Self-starting 'ode' solvers, subroutines 'ode45' and 'ode15s', of MATLAB® were examined. Several particle trajectories were computed and their final position after a single breathing cycle was compared with their initial position based on absolute tolerance of 10^{-16} and relative tolerance of 10^{-8}. We picked the more accurate, albeit more time consuming, ode15s that introduced a maximum error of order $10^{-6} R_1$ in particle position.

The program was run during five hundred breathing cycles and both trajectories and Poincaré maps, based on sampling particle physical location after each breathing cycle, were obtained. The results illustrate the rich behaviour of massless particle motion for which periodic, quasi-periodic and chaotic trajectories may exist.

In figures 7 to 12 the following dimensionless geometrical parameters were employed: $\overline{R}_2 = 0.3$, $\varepsilon = 0.525$, which yield a single separation surface between the flow near the inner cylinder and the flow inside the wide gap (rotation only case). From figure 7

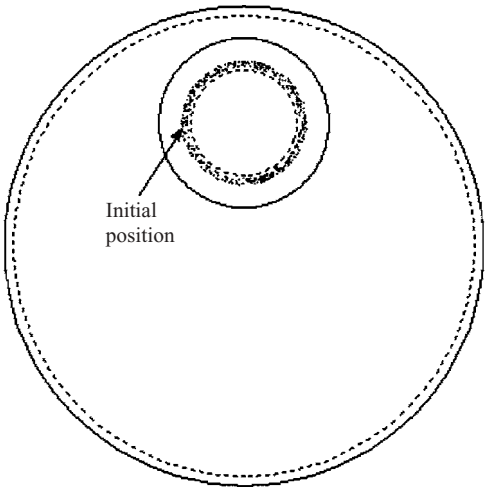

FIGURE 8. As figure 7 but for a single particle introduced initially near the inner cylinder at $(\eta_i, \xi_i) = (1.5, \pi/3)$. Chaotic behaviour can again be observed.

onward the broken and full circles show the cylinder's walls at the onset of inhalation and exhalation, respectively. In figures 7 to 9 we assume that $R_1 = 1 - 0.02\cos(2\pi\tau)$, breathing protocol A, and $\Omega T = 20$ associated with $\gamma \approx 1700$, or airway generation 18, according to (23). Here $\tau = t/T$ is the dimensionless time. The phase angles used are $\delta_1 = \pi/18$ and $\delta_2 = (5/6)\pi$ (see figure 6) so that the breathing process has unequal inhalation and exhalation time periods. In figure 7, a single particle is introduced initially at $(\eta_i, \xi_i) = (0.6, \pi/3)$ and its path is computed during 500 cycles. Its location is sampled after every breathing period to derive a simplified depiction of its behaviour. The Poincaré map thus obtained illustrates that the particle wanders within a large area between the cylinders with a characteristic stochastic behaviour. It leaves and enters the alveolus, spending part of its time in the adjacent airway with an obvious exclusion of a small region encompassing the stagnation point. In figure 8 a particle that is initially placed near cylinder 2 at $(\eta_i, \xi_i) = (1.5, \pi/3)$ creates a thin stochastic layer, never leaving that area during the 500 cycles. That is, the particle never enters the alveolus. However, in figure 9(a), remarkable, quasi-periodic tori of order 4 are obtained for a particle initially placed at $(\eta_i, \xi_i) = (0.8, 0)$, a location inside the unvisited region observed in figure 7. In figure 9(c) this particle's trajectory during the 500 breathing cycles is also illustrated, reaffirming its quasi-periodic nature. In figure 10 a four-fold lower value of the parameter $\Omega T = 5$ that is associated with $\gamma \approx 420$, and represents an alveolus located at airway generation 21, was examined. A particle was placed at $(\eta_i, \xi_i) = (0.6, \pi/3)$ and again a chaotic map was obtained, revealing that the particle never left the alveolus. However, in figure 11 for which the parameter $\Omega T = 1$ is further reduced (representing generation 22 with $\gamma \approx 85$) a particle initially placed at the same location, namely at $(\eta_i, \xi_i) = (0.6, \pi/3)$, undergoes only a quasi-periodic motion. Figure 11(b, c) that illustrates the time evolution of η, ξ and the particle trajectory reaffirms this conclusion. These last results indicate the importance of the alveolus' location along the acinar tree, affecting, for instance, mixing efficiencies, as shall be shown later.

In figure 12(a) time protocol B (figure 6) is employed with $\delta = \pi/18$ representing a characteristic sinusoidal breathing process. The particle is initially again placed at $(\eta_i, \xi_i) = (0.6, \pi/3)$, with $\Omega T = 20$. Once again a chaotic behaviour is observed where

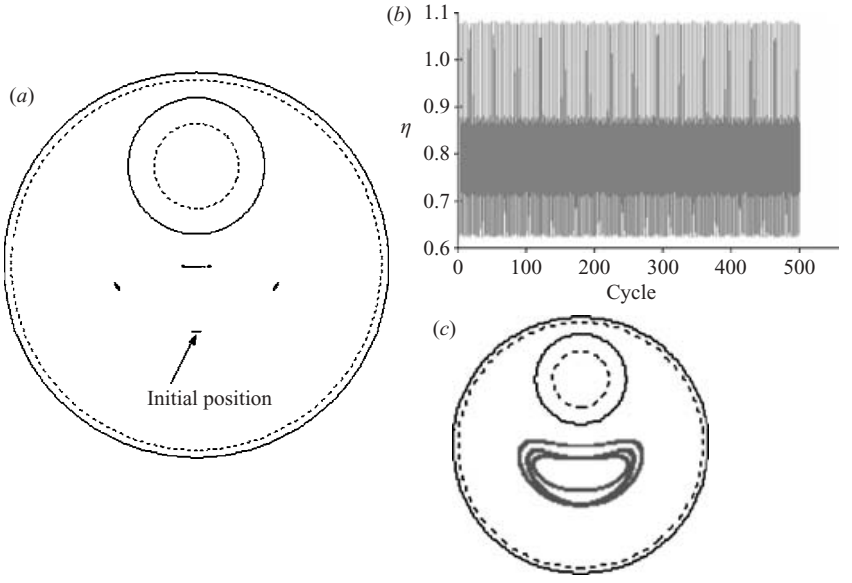

FIGURE 9. (*a*) Poincaré map for a single particle introduced initially at $(\eta_i, \xi_i) = (0.8, 0)$ and its position sampled after each breathing period during 500 breathing cycles. Quasi-periodic tori of order 4 are obtained. Rotation of inner cylinder is according to protocol A (figure 6) with $\delta_1 = \pi/18$ and $\delta_2 = 5\pi/6$ and $\Omega T = 20$ associated with airway generation 18. The geometrical configuration is defined in figure 5, where the dotted and full circles pertain to the minimum and maximum size of the cylinders at the onset of inhalation and exhalation, respectively. (*b*) Time evolution of η and (*c*) trajectory of the particle that illustrates its quasi-periodic motion.

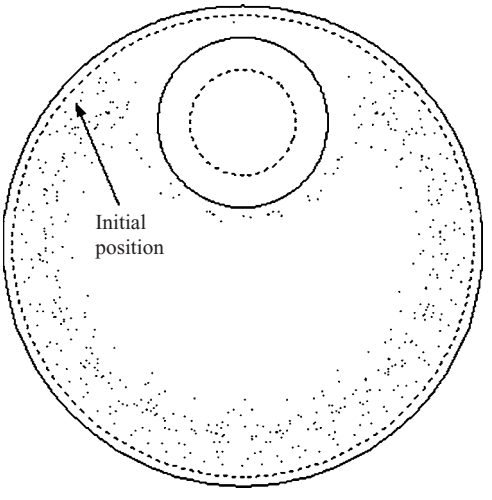

FIGURE 10. Poincaré map of a particle defined in figure 7 with $\Omega T = 5$ associated with airway generation 21. Chaotic behaviour is observed.

the particle samples locations within both the airway and the alveolus, generally similar to the result shown in figure 7, with a somewhat larger region unvisited. Figure 12(b, c) reaffirms this conclusion, showing the time evolution of η, ξ and particle trajectory during 500 breathing cycles. This result reaffirms the conclusion reached by Haber *et al.* (2000) who also used time protocol B.

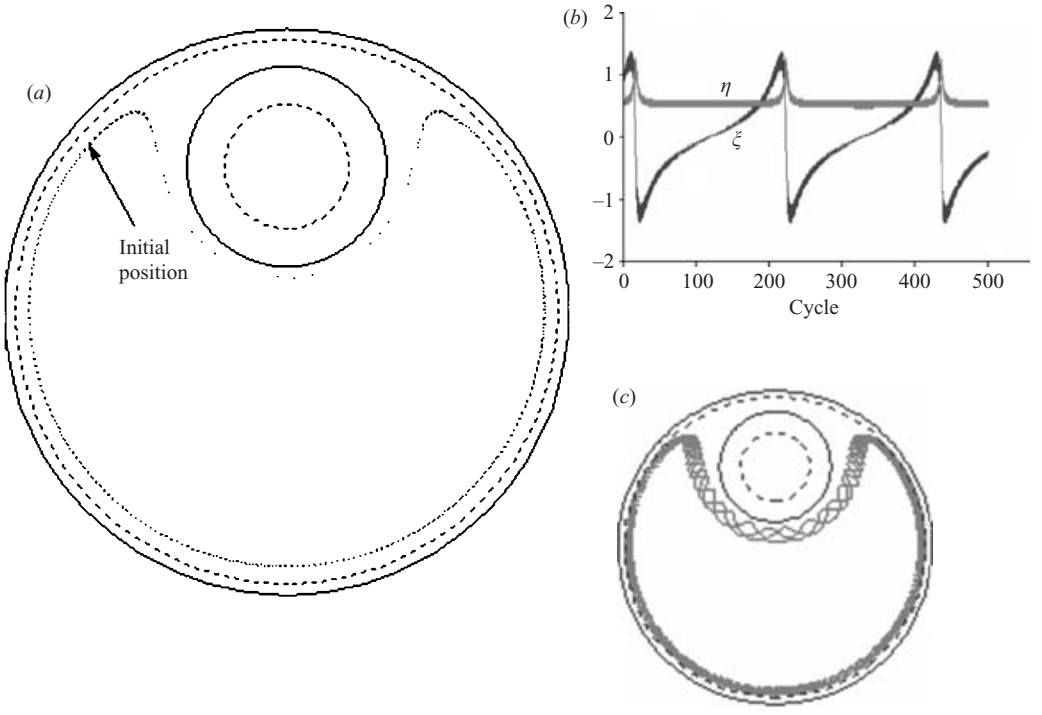

FIGURE 11. (*a*) Poincaré map of a particle defined in figure 7 with $\Omega T = 1$ associated with airway generations 22, 23. (*b*) Time evolution of η and ξ. (*c*) Particle trajectory. Quasi-periodic motion is observed.

A different parameter set was employed for figures 13 to 18 where $\overline{R}_2 = 0.5$, $\varepsilon = 0.4$ and $R_1 = 1\text{–}0.05\cos(2\pi\tau)$ with the higher alveolar expansion ratio $\beta = 0.05$. In this case the appearance of a saddle point (for $\delta = 0$ and equal inhalation and exhalation periods) occurs at about $\gamma = 300$. Figure 13(*a*) illustrates the simultaneous behaviour of 20 particles placed initially along the straight line defined by $\xi = 0$ and π, at equal intervals in η (from $\eta = 0.63$ to 1.1). The sinusoidal time protocol B was employed during 500 cycles with lag angle $\delta = \pi/18$ and $\Omega T = 4\,(\gamma = 400)$. A small area of chaos exists near the cylinder walls and quasi-periodic orbits survive in most of the domain occupied by the alveolus. A similar behaviour with a larger area of chaos inside the alveolus domain is shown in figure 13(*b*) where a higher value of shear $\Omega T = 20$ ($\gamma = 2000$) was employed. A completely different Poincaré map is shown in figure 14 for a small value of shear $\Omega T = 0.5$ ($\gamma = 50$). The chaotic region disappears and quasi-periodic orbits dominate the behaviour of a massless tracer.

In conclusion, the effect of unequal inhalation and exhalation periods leads to chaotic behaviour, similar to the case in which a sinusoidal time lag between breathing and expansion is assumed. The appearance of chaos under slight disturbances of δ and uneven durations of inhalation and exhalation is intimately connected to the appearance of a saddle point. The effect of γ on mixing is more complex and will be dealt with separately in the following subsection.

3.2. *Mixing*

The investigation of mixing and its quantification is carried out for particles about 0.2 μm to 1 μm in diameter that are in abundance, for instance, in cigarette smoke,

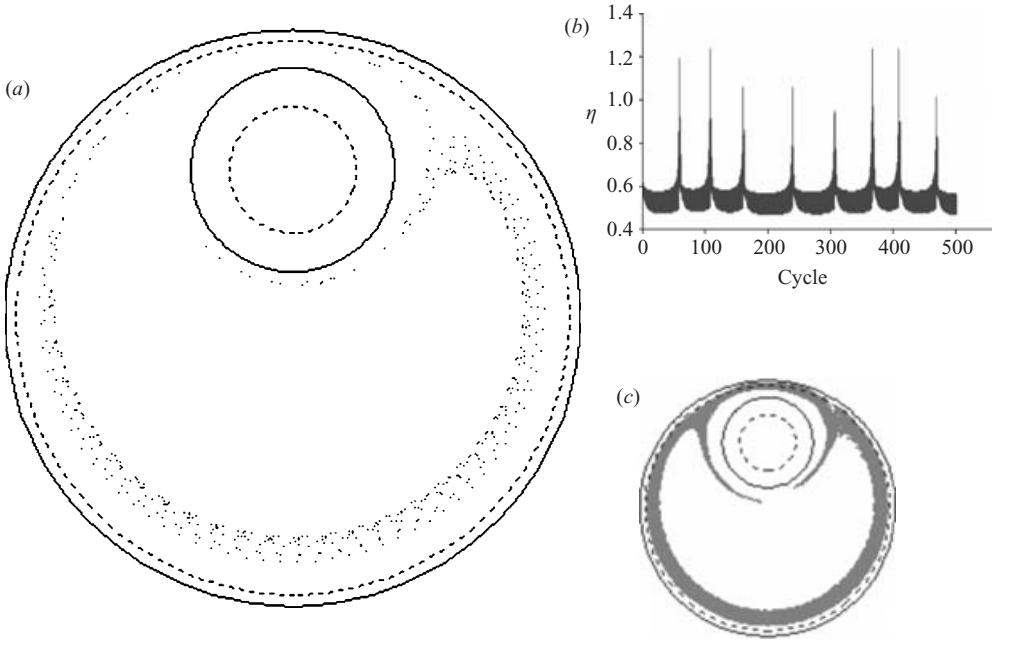

FIGURE 12. (*a*) Poincaré map for a single particle introduced initially at $(\eta_i, \xi_i) = (0.6, \pi/3)$ and its position sampled after each breathing period during 500 breathing cycles. Chaotic behaviour can be observed. Rotation of inner cylinder is according to Protocol B (figure 6) with $\delta = \pi/18$ and $\Omega T = 20$ associated with airway generation 18. The geometrical configuration is defined in figure 5, where the dotted and full circles pertain to the minimum and maximum size of the cylinders at the onset of inhalation and exhalation, respectively. (*b*) the time evolution of η and (*c*) Trajectory of a particle is also shown elucidating the chaotic behaviour of such a particle.

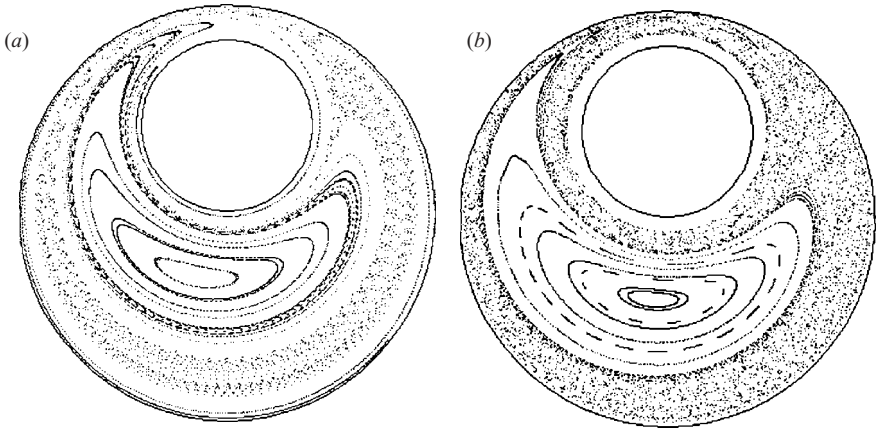

FIGURE 13. Poincaré map for 20 particles initially placed at $\xi = 0$, π and $\eta = 0.63$ to 1.1 at 10 equally spaced η locations. Narrow chaotic regions near the walls and wider chaotic regions that occupy a larger region of the alveolus domain can be observed for cases (*a*) and (*b*), respectively. The sinusoidal time protocol B was employed with $\delta = \pi/18$, $S/\pi = 0.75$, $\varepsilon = 0.4$, $\beta = 0.05$ for (*a*) $\Omega T = 4$ and (*b*) $\Omega T = 20$.

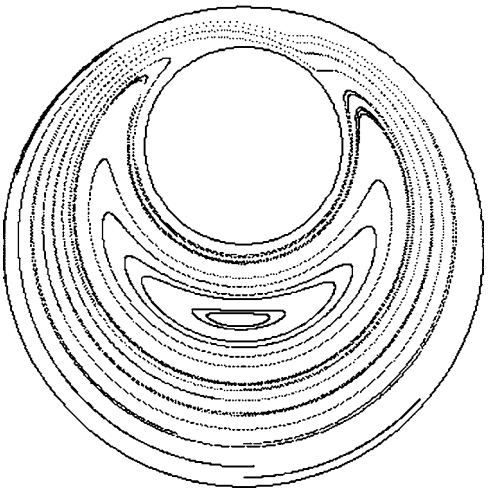

FIGURE 14. As figure 13 but for $\Omega T = 0.5$. No chaotic regions are observed and the space is dominated by quasi-periodic orbits.

and have prominent physiological effects. Generally, for particles in this size range, Brownian motion, gravitational sedimentation and particle inertia are considered to be less significant than particle convection†, originated by the alveolar flow, in particular at the proximal region of the acinar tree. Nevertheless, whereas particles which experience chaotic advection in Hamiltonian systems are confined to or by KAM tori and cantori, small-scale processes such as Brownian motion or gravitational sedimentation may enable particles to cross such boundaries without hindrance. Consequently it is conceivable that even fairly weak intrinsic motion might disrupt chaotic advection; particles might move between regions where the flow is chaotic and regions where it is regular. These combined effects, that have still to be explored, have not been addressed in this study.

Mixing of much finer or ultrafine particles are strongly affected by Brownian motion, particularly at the distal regions of the acinar tree.

In the following analysis, we focus on mixing processes directly related to quasi-periodic and chaotic motion of the particles. The cyclic analytical model proposed here lends itself to a relatively easy computation of the overall mixing efficiency. A well-defined norm that may quantify local instantaneous mixing in hydrodynamic systems is directly correlated to the value of the second invariant of the shear rate tensor $\boldsymbol{S}:\boldsymbol{S}$ where

$$\boldsymbol{S} = 0.5(\nabla \boldsymbol{v} + \nabla \boldsymbol{v}^T). \tag{26}$$

An instantaneous measure of mixing rate M in the system as a whole,

$$M = 2 \int_V (\boldsymbol{S}:\boldsymbol{S})\, \mathrm{d}V, \tag{27}$$

† For instance, if we consider a 0.5 μm particle, its diffusion coefficient at body temperature is about $6.8 \times 10^{-11}\,\mathrm{m^2\,s^{-1}}$. The diameter of a typical alveolus is about 200 μm. The fluid velocity varies depending upon breathing frequency and the location of the alveolus along the acinar tree. For a typical breathing period of 5 s and alveoli at the 16th generation, the velocity scale inside the alveoli is about $0.03\,\mathrm{cm\,s^{-1}}$ and consequently the Péclet number is about 440. At the 22nd generation it decreases to about 7. The effects of sedimentation due to gravity and particle inertia are even smaller.

is proportional to the rate of energy dissipation, where V is the volume occupied by the fluid. This definition is based on the notion that the rate of energy dissipation, intimately linked with the rate of entropy production, is directly correlated with the amount of disorder required to obtain a well-mixed system. Thus, it seems that the higher the value of M the better the mixing. This rather simplified view, addressed later in more detail, may lead to erroneous results if not applied carefully.

Notice that the definition of M based on $\boldsymbol{S}:\boldsymbol{S}$, rather than the more common $(\boldsymbol{S}:\boldsymbol{S})^{1/2}$‡, greatly simplifies its evaluation. By a simple application of the Gauss theorem the following identity can easily be proven:

$$M = 2\int_V (\boldsymbol{S}:\boldsymbol{S})\,\mathrm{d}V = \frac{1}{\mu}\int_A (\boldsymbol{n}\cdot\boldsymbol{\sigma}\cdot\boldsymbol{v})\,\mathrm{d}A, \tag{28}$$

where A is the surface area bounding the volume V and $\boldsymbol{n}$ is a unit vector perpendicular to A and pointing outward from V.

Henceforth, we shall address the case of a single alveolus and the adjacent airway. Thus, according to our model, the volume of the system pertains to the space bounded by the two cylinders. In this case the velocity on the boundary A is a known constant quantity and the evaluation of M entails a simple evaluation of the stress tensor $\boldsymbol{\sigma}$ at the surface A. Notice that in our case A includes the surfaces $A_1 + A_2$ of the outer and inner cylinders (per unit length), respectively, for which

$$\left.\begin{aligned} &\boldsymbol{n}_1 = -\boldsymbol{i}_\eta, \quad \boldsymbol{n}_2 = \boldsymbol{i}_\eta, \quad \mathrm{d}A_1 = \frac{c}{\cosh\eta_1 - \cos\xi}\,\mathrm{d}\xi, \quad \mathrm{d}A_2 = \frac{c}{\cosh\eta_2 - \cos\xi}\,\mathrm{d}\xi \\ &\boldsymbol{v}|_{A_1} = -\boldsymbol{i}_\eta U_1, \quad \boldsymbol{v}|_{A_2} = -\boldsymbol{i}_\eta U_2 + \boldsymbol{i}_\xi \Omega_2 R_2 \quad V = \pi\left(R_1^2 - R_2^2\right). \end{aligned}\right\} \tag{29}$$

Substitution of (29) into (28) yields

$$M = \frac{c}{\pi\mu}\left[U_1\int_{-\pi}^{\pi}\frac{\sigma_{\eta\eta}(\eta=\eta_1)}{\cosh\eta_1 - \cos\xi}\,\mathrm{d}\xi - U_2\int_{-\pi}^{\pi}\frac{\sigma_{\eta\eta}(\eta=\eta_2)}{\cosh\eta_2 - \cos\xi}\,\mathrm{d}\xi + \Omega_2 R_2\int_{-\pi}^{\pi}\frac{\sigma_{\xi\eta}(\eta=\eta_2)}{\cosh\eta_2 - \cos\xi}\,\mathrm{d}\xi\right]. \tag{30}$$

The general expressions for the stress components $\sigma_{\eta\eta}$ and $\sigma_{\xi\eta}$ in terms of the stream function are

$$\begin{aligned} \sigma_{\eta\eta} + p &= -\sigma_{\xi\xi} - p \\ &= -\frac{2\mu}{c^2}(\cosh\eta - \cos\xi)\left[(\cosh\eta - \cos\xi)\frac{\partial^2\Psi}{\partial\xi\,\partial\eta} + \sin\xi\frac{\partial\Psi}{\partial\eta} + \sinh\eta\frac{\partial\Psi}{\partial\xi}\right], \quad (31a) \\ \sigma_{\xi\eta} &= \frac{\mu}{c^2}(\cosh\eta - \cos\xi)\left[(\cosh\eta - \cos\xi)\left(\frac{\partial^2\Psi}{\partial\eta^2} - \frac{\partial^2\Psi}{\partial\xi^2}\right) + 2\sinh\eta\frac{\partial\Psi}{\partial\eta} - 2\sin\xi\frac{\partial\Psi}{\partial\xi}\right]. \quad (31b) \end{aligned}$$

Introduction of (5), (6c), (12), (15c), (16), (17) into (31) and (30) yields, after some tedious algebra, the following simple expression for M:

$$\begin{aligned} M = {} & 2\pi\Omega^2 R_2^2[C_0\cosh(\eta_2) + D_0\sinh(\eta_2)] + 4\pi U^2[(\eta_2 - \eta_1)\sinh(\eta_2 - \eta_1)/\Delta_1 \\ & - 0.5(\mathrm{e}^{-2\eta_1} - \mathrm{e}^{-2\eta_2}) + \sinh(\eta_2 - \eta_1)\sinh(\eta_2 + \eta_1)], \end{aligned} \tag{32}$$

where C_0, D_0 and Δ_1 are defined in Appendix A with $\Omega_1 = 0$ and $\Omega_2 = \Omega$.

‡ In the past we (Haber *et al.* 2000) and others (e.g. Ottino 1989) have used $(\boldsymbol{S}:\boldsymbol{S})^{1/2}$ to scale local instantaneous mixing. The difference is not fundamental since both quantities are positive definite.

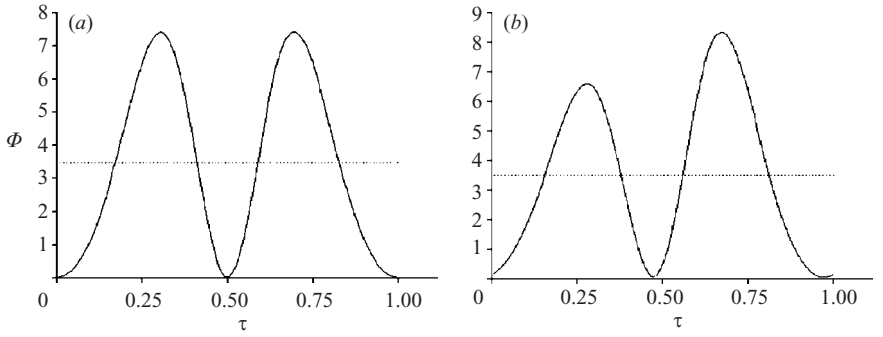

FIGURE 15. (*a*) Specific mixing for time protocol B with $\Omega T = 2$ and phase angle $\delta = 0$. A two- hump distribution was obtained, symmetric with respect to $t/T = 0.5$. (*b*) As (*a*) but with phase angle $\delta = 10^{\circ}$. A two- hump distribution can be observed but Φ is no longer symmetric, a mark of irreversibility.

Figures 15(*a*) and 15(*b*) illustrate the specific mixing $\Phi = M/[\pi(R_1^2 - R_2^2)]$ during a single breathing cycle, a parameter that is independent of the system size. Time was scaled with the inverse of the breathing frequency $1/T$. In figure 15(*a*) we used the time protocol B with phase angle $\delta = 0$ and $\Omega T = 2$. A two-hump distribution was obtained, symmetric with respect to $t/T = 0.5$. This symmetry is a direct outcome of the flow reversibility of Stokes flows. However, in the case in which a phase lag exists between ductal flow (rotation) and the expansion of the alveolus, inhalation and exhalation no longer lead to reversible processes. This is shown in figure 15(*b*) for which a phase angle of $\delta = \pi/18$ and $\Omega T = 2$ is applied. A two-hump distribution can still be observed but Φ is no longer symmetric, a mark of the foregoing irreversibility.

If M represents a measure of the instantaneous mixing rate that also accounts for the system size, the extent of mixing increases with Ω. As we shall show later this result is rather simplistic since it does not represent the overall extent of mixing in a system during an entire breathing period. Such a quantity, $\overline{M}$, can be defined by calculating the temporal average of M over a single breathing period T,

$$\overline{M} = \frac{1}{T} \int_T M \, \mathrm{d}t. \tag{33a}$$

This definition results in a dimensional value. A dimensionless scale that may better represent the extent of mixing per unit cycle is

$$E = \frac{1}{V^{1/2}} \int_T M^{1/2} \, \mathrm{d}t. \tag{33b}$$

However, this expression cannot distinguish between reversible and irreversible flows. For instance, when periodic flows with zero mean are applied, e.g. a case in which the inhalation and exhalation processes are exactly reversible, every unit volume inside the system returns to its initial shape after a full breathing period and, in essence, no lasting mixing occurs. Expressions (33*a*) or (33*b*), however, predict non-zero positive values regardless of flow reversibility. This example demonstrates that the rather sensible approach, linking generation of energy dissipation or entropy production with disorder and mixing efficiency, may result in erroneous conclusions, particularly in nearly periodic Stoksian fields. A possible method to circumvent this difficulty is to introduce a 'Poincaré shear rate', the symmetric part of the displacement gradient tensor after a full breathing cycle (Haber *et al.* 2000), that

replaces the normally defined $\boldsymbol{S}$. Thus, a unit time is replaced by a unit cycle. In this case, fully reversible flows will result in zero $\boldsymbol{S}$, and, consequently, a zero value of M will be obtained. However, 'Poincaré shear rates' are not easily calculated and pose a formidable analytical task in our case (one needs to integrate (25) from $t=0$ to $t=T$).

We suggest a novel and much simpler method for scaling an 'overall extent of mixing' per unit cycle that is parameter P dependent and that subtracts unwanted effects of flow reversibility, namely,

$$E^P = \frac{1}{V^{1/2}} \left| \left(\int_T M^{1/2} \mathrm{d}t \right)_{P=\{P_{Rev}+\Delta P\}} - \left(\int_T M^{1/2} \mathrm{d}t \right)_{P=\{P_{Rev}\}} \right|, \tag{33c}$$

where ΔP is a perturbation to P. Here, the second integral employs a basic set of parameters $\{P_{Rev}\}$ yielding reversible inhalation and exhalation flows while the first integral is evaluated for a finite perturbation of a single parameter P. For example, in our case we know that a basic parameter set that yields reversibility requires that $\delta=0$ and that inhalation and exhalation times are equal. However if δ is not zero (we shall assume the physiologically observed value of $\delta=\pi/18$), quasi-periodicity or chaos can be expected and inhalation and exhalation do not induce reversible flows.

Overall mixing efficiencies for various values of ΩT and system configurations were examined with a perturbation parameter $\delta=\pi/18$. The reversible set chosen included $P_{Rev}=\{$time protocol B, $R_0=1$, $\beta=0.05$, $S/\pi=0.75$, $\varepsilon=0.4$, $\delta=0\}$. For $\beta=0$ (no expansion) all of the above reversible sets generate a streamline map similar to that illustrated in figure 1(*c*). It includes a separation surface that divides the flow field into two distinct regions and a stagnation point inside the wide gap region.

Calculating the overall mixing efficiency dependence on γ revealed a striking pattern. A typical case is provided in figure 16. We normalized the results with the value of E_{16}^{δ} (the extent of overall mixing at the 16th airway generation) to mark the relative mixing efficiency of the various generations. The figure illustrates that the extent of mixing is zero for zero values of γ (or Ω), corresponding to the most distal end of the acinar tree, generation 23, it increases to a local maximum, corresponding to generation 22, and decreases to a local minimum for a $\gamma_{\min}$ value about 300 (generation 21). It increases steadily again, almost linearly, with higher values of γ. This result is counter-intuitive since it seems that mixing should increase monotonically with γ, the argument being that higher rotations (shear-induced flow) induce stronger stretching and rotations of fluid elements, resulting in better mixing. This view is, however, contradicted by our results and it seems that two competing mechanisms determine the overall extent of mixing. The first mechanism plays a significant role when γ values are low ($<\gamma_{\min}$) and the second plays a predominant role when γ values are larger than $\gamma_{\min}$. A careful examination of the streamline maps of all the above-mentioned configurations reveals that the appearance of a saddle point and of a homoclinic orbit occurs at $\gamma\approx\gamma_{\min}$. It is well accepted that chaotic behaviour of a system and the appearance of saddle points and homoclinic orbits are intimately related. Thus, it is very likely that once chaos occurs the overall extent of mixing increases for the γ range $\gamma>\gamma_{\min}$. However, for γ values lower than $\gamma_{\min}$ trajectories of the majority of fluid particles would exhibit quasi-periodic behaviour (see for example figure 14) and a different kinematic mixing mechanism becomes predominant. A possible explanation of this mechanism is based on the following observations: flow induced solely by either periodic rotation or by periodic expansion is exactly reversible and thereby would yield zero overall mixing if operated

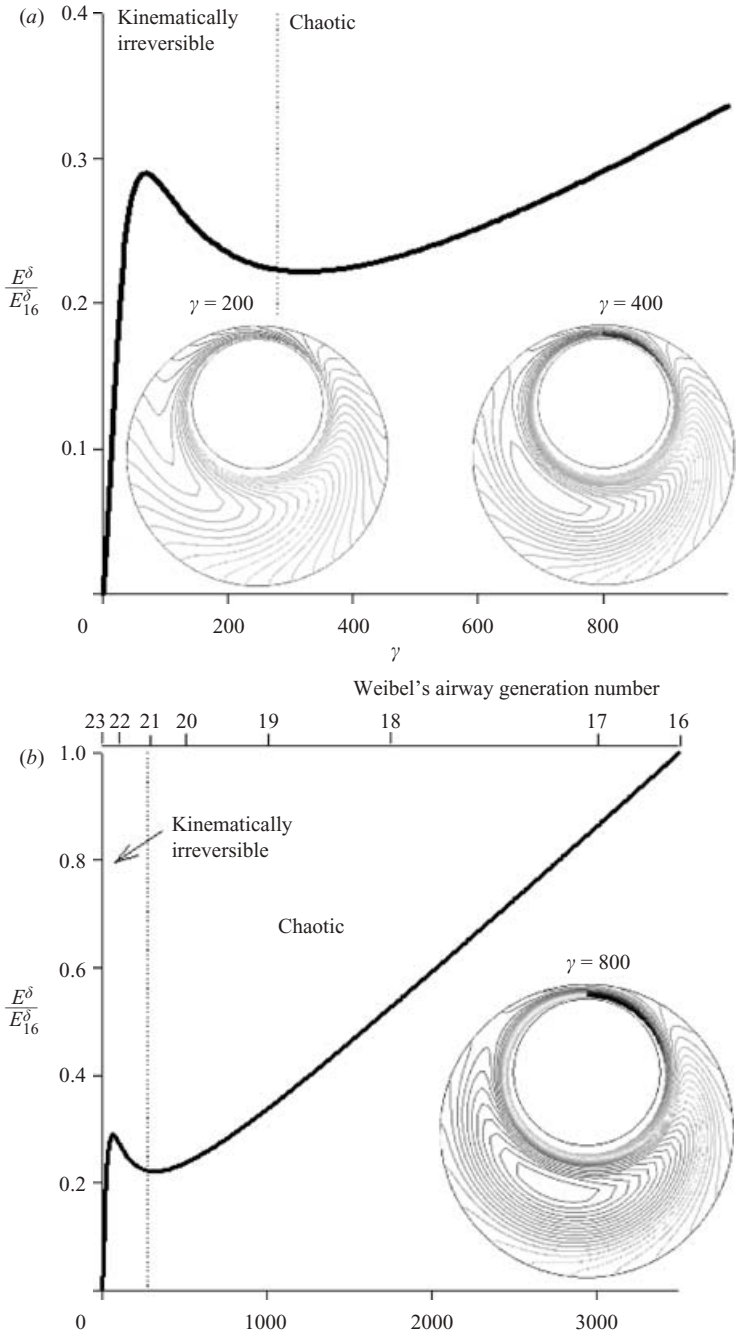

FIGURE 16. Mixing efficiency as a function of the angular velocity associated with airway generation via the equation $\gamma = 100\Omega T$. The reversible set is $P_{rev} = \{$time protocol A, $R_0 = 1$, $\beta = 0.05$, $S/\pi = 0.75$, $\varepsilon = 0.4$, $\delta = 0\}$. Near zero values of γ pertaining to the lowest end of the acinar tree, generation 23, the overall mixing efficiency is small but is rapidly increasing to a local maximum value at about $\gamma = 70$ that pertains to generation 22 and then decreases to a local minimum at generation 21 (at about $\gamma = 320$) and increases again up the acinar tree.

separately. Only a combination of these two rhythmical out-of-phase motions would induce kinematically irreversible motion, manifested by the quasi-periodic orbits of the fluid particles, and consequently mixing. Indeed, if one of the rhythmical motions dominates the flow, it becomes nearly reversible (when Ω is small expansion dominates and when Ω is relatively high the shear-induced flow dominates). Consequently, irreversibility is highest at an intermediate value between zero and $\gamma_{\min}$, and mixing is most pronounced for intermediate values of Ω in this region. We believe that this reversible/irreversible mechanism results in the local minimum and maximum observed in figure 16. It should be noted that Brownian motion of fine particles must be considered and, consequently, its effect on mixing must be accounted for, especially for low values of $\gamma(<\gamma_{\min})$ representing the smallest airways.

It should also be clear that the overall extent of mixing, so defined, pertains to a single alveolus at a certain location down the acinar tree. It by no means reflects a global mixing efficiency of the acinus. An obvious extension of the foregoing to the whole lung is straightforward. If the total number of alveoli attached to all airways of generation i is N_i, the instantaneous extent of mixing (defined in (27)) of a single alveolus of volume V_i is M_i. If M_{acinus} denotes the corresponding value for the whole acinus of volume $V_{acinus} = \sum N_i V_i$, then

$$M_{acinus} = \sum_{16}^{23} M_i N_i \tag{34a}$$

and

$$E^P_{acinus} = \frac{1}{V^{1/2}_{acinus}} \left| \left(\int_T M^{1/2}_{acinus} \mathrm{d}t \right)_{P=\{P_{Rev}+\Delta P\}} - \left(\int_T M^{1/2}_{acinus} \mathrm{d}t \right)_{P=\{P_{Rev}\}} \right|. \tag{34b}$$

For regular perturbations for which the following limit exists, we may also define 'sensitivity of mixing to a parameter P' as

$$s^P = \lim_{\Delta P \to 0} \frac{1}{V^{1/2}} \frac{\left| \left(\int_T M^{1/2} \mathrm{d}t \right)_{\{P_{Rev}+\Delta P\}} - \left(\int_T M^{1/2} \mathrm{d}t \right)_{\{P_{Rev}\}} \right|}{\| \Delta P \|} \tag{35}$$

where in this case a certain parameter, say P, is perturbed by an infinitesimally small value ΔP to investigate the sensitivity of the overall extent of mixing to variations of this parameter.

To calculate mixing sensitivity to phase angle δ we use the foregoing reversible parameter set and calculate s^δ according to (35) for increasingly smaller values of δ. Figure 17 depicts mixing sensitivity (per δ in degrees) for various values of ΩT. An almost linear increase is obtained except for ΩT values less than 0.2 (see inset). This reflects the regular dependence of E^δ on the phase angle δ according to time protocol B (figure 6*b*).

4. Summary

A simple model for the lung alveoli is suggested that consists of fluid bounded by walls of two eccentric cylinders that perform periodic expansion and periodic rotation (of the inner cylinder only). The former mimics the expansion of an alveolus while the latter generates the shear flow that exists inside an airway adjacent to the alveolus. Varying the angular velocity of the inner cylinder makes it possible to imitate the

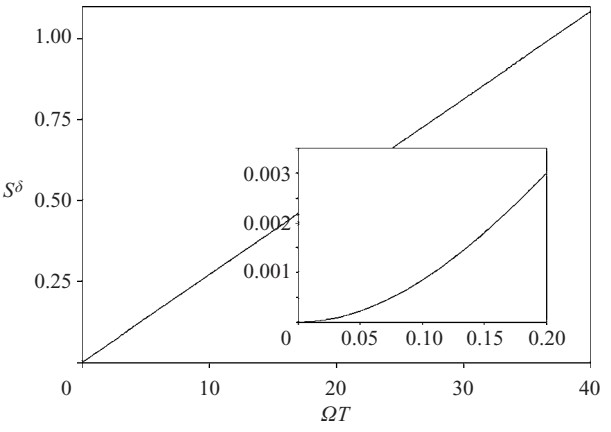

FIGURE 17. Mixing sensitivity (per δ in degrees) for various values of ΩT. An almost linear increase is obtained that reflects the regular dependence of E^δ upon the phase angle δ according to time protocol B (figure 6).

flow induced within alveoli attached to different airway generations down the acinar tree.

Poincaré maps were drawn for which a fluid particle location was sampled after every breathing period. These reveal that chaos may exist when either: (i) a phase angle exists between the periodic motions of cylinder expansion and of rotation, similar to the flow generated by alveolus expansion and airway flow, or, (ii) inhalation and exhalation durations are not identical. Quasi-periodic and chaotic patterns may co-exist depending on the initial location inside the alveolus and the ratio γ between shear- and expansion-induced flows. Quasi-periodic trajectories are mainly observed near the centre region of the alveolus (where a stagnation point exists for non-expanding cylinders) while chaotic patterns begin near the walls, namely, near the alveolus mouth and its boundary where stretching and folding due to shear and expansion are the strongest.

An easily calculated measure of the overall extent of mixing that disregards unwanted reversible flows was suggested. The dependence of the mixing on γ exhibits a 'strange' counter-intuitive behaviour: an increase to a local maximum, a decrease to a local minimum and a steady monotonic increase as γ increases. (A local maximum and minimum occur at the 22nd and 21st generations, respectively. Then, the mixing efficiency increases monotonically as we move to more proximal generations of the acinar tree.) This behaviour can be attributed to two different mechanisms: for small values of γ (between zero and that yielding a minimum extent of mixing) a reversibility/irreversibility mechanism dominates the flow while for high γ values the flow becomes chaotic and mixing is enhanced. Consequently, poor mixing is expected inside alveoli placed at the 23rd generation since the recirculation zone in the model is largely filled with KAM tori. No mixing occurs if the phase angle δ between the rhythmical shear- and expansion-induced flows is zero. It is enhanced monotonically as δ increases. We have also defined mixing sensitivity with respect to an operational parameter and have shown that the overall extent of mixing with respect to the phase angle δ decays monotonically with airway generation number.

Finally, we would like to point out several drawbacks of this model: the flow is solved in a two-dimensional rather than in the three-dimensional space in which the

actual flow takes place; the flow near the inner cylinder represents just the shear part of the actual flow inside the airway adjacent to the mouth of the alveolus; the length of the narrow gap representing the short duct connecting adjacent alveoli cannot be controlled whereas in a real acinar tree the alveoli at the highest generations may practically touch; the 23rd generation alveoli might be interconnected rather than attached to an adjacent airway; Brownian motion and its effect on mixing was excluded. The coupling of convective, diffusive and gravitational forces and their effect on mixing still awaits exploration.

Despite the foregoing limitations, we believe that the qualitative nature of the flow in the alveolus region, by far the most interesting region, is faithfully simulated by this simple model.

This research was supported by the Fund for The Promotion of Research at The Technion, and National Heart, Lung and Blood Institute Grant NIH HL054885, H1070542, and HL074022.

Appendix A

The general expressions for coefficients defined in (5) that also include rotation of cylinder 1 possess the following general form (we use the abbreviations 'sh' for 'sinh' and 'ch' for 'cosh'):

$$A_0 = \frac{1}{\Delta_0}\left[E(\mathrm{ch}\eta_1\mathrm{ch}\eta_2\mathrm{sh}\eta_{21} - \eta_1\mathrm{ch}^2\eta_2 + \eta_2\mathrm{ch}^2\eta_1) - \frac{\Omega_1 R_1}{\Omega_2 R_2}(\eta_2\eta_{21}\mathrm{ch}\eta_1 - \eta_1\mathrm{ch}\eta_2\mathrm{sh}\eta_{21})\right.$$
$$\left. -(-\eta_1\eta_{21}\mathrm{ch}\eta_2 + \eta_2\mathrm{ch}\eta_1\mathrm{sh}\eta_{21})\right],$$

$$B_0 = \frac{1}{\Delta_0}\left\{0.5E[\eta_{21}(\eta_2+\eta_1) + \eta_1\mathrm{sh}(2\eta_2) - \eta_2\mathrm{sh}(2\eta_1) - \mathrm{sh}(\eta_1+\eta_2)\mathrm{sh}\eta_{21}] - \frac{\Omega_1 R_1}{\Omega_2 R_2}\right.$$
$$\left.\times(-\eta_2\eta_{21}\mathrm{sh}\eta_1 + \eta_1\mathrm{sh}\eta_2\mathrm{sh}\eta_{21}) - (\eta_1\eta_{21}\mathrm{sh}\eta_2 - \eta_2\mathrm{sh}\eta_1\mathrm{sh}\eta_{21})\right\},$$

$$C_0 = \frac{1}{\Delta_0}\left[E\mathrm{sh}(\eta_1+\eta_2)\mathrm{sh}\eta_{21} - \frac{\Omega_1 R_1}{\Omega_2 R_2}(-\eta_{21}\mathrm{ch}\eta_1 + \mathrm{ch}\eta_2\mathrm{sh}\eta_{21}) - (\eta_{21}\mathrm{ch}\eta_2 - \mathrm{ch}\eta_1\mathrm{sh}\eta_{21})\right],$$

$$D_0 = \frac{1}{\Delta_0}\left\{E[-\eta_{21} - \mathrm{ch}(\eta_1+\eta_2)\mathrm{sh}\eta_{21}] - \frac{\Omega_1 R_1}{\Omega_2 R_2}(\eta_{21}\mathrm{sh}\eta_1 - \mathrm{sh}\eta_2\mathrm{sh}\eta_{21})\right.$$
$$\left. -(-\eta_{21}\mathrm{sh}\eta_2 - \mathrm{sh}\eta_1\mathrm{sh}\eta_{21})\right\},$$

$$A_1 = E\mathrm{ch}(\eta_1+\eta_2)/\Delta_1, \quad B_1 = -E\mathrm{sh}(\eta_1+\eta_2)/\Delta_1,$$
$$C_1 = E(\eta_1+\eta_2)\mathrm{ch}\eta_{21}/\Delta_1, \quad D_1 = -2E\mathrm{ch}\eta_{21}/\Delta_1,$$

where

$$\eta_{21} = \eta_2 - \eta_1, \quad \Delta_0 = \mathrm{sh}^2\eta_{21} - \eta_{21}^2, \quad \Delta_1 = 2(\eta_{21}\mathrm{ch}\eta_{21} - \mathrm{sh}\eta_{21}),$$
$$E = \frac{\left[\frac{\Omega_1 R_1}{\Omega_2 R_2}(\eta_{21}\mathrm{sh}\eta_1 - \mathrm{sh}\eta_2\mathrm{sh}\eta_{21}) + (-\eta_{21}\mathrm{sh}\eta_2 + \mathrm{sh}\eta_1\mathrm{sh}\eta_{21})\right]}{[2\mathrm{ch}\eta_{21}\Delta_0/\Delta_1 + \eta_{21} + \mathrm{sh}\eta_{21}\mathrm{ch}(\eta_1+\eta_2)]}.$$

In our lung model we assume the particular case in which $\Omega_1 = 0$. Thus, all the foregoing coefficients depend solely on η_1 and η_2. It can also easily be proven that $Ec\Omega_2 R_2$ is the total flow rate passing through the gap between the rotating cylinders.

Note that the foregoing expressions differ in appearance from those given by Ballal & Rivlin (1976). To validate our results and the numerical procedures later employed, we tested the most complex case in which the eccentricity is large and both Ω_1 and Ω_2 are non-zero. The agreement with the streamline map shown by Aref (1984) was excellent.

Appendix B

The stream function (17)

$$\Psi = c(U\psi^{EXP} + \Omega_2 R_2 \psi^{ROT}) \equiv H \tag{B 1}$$

can also be viewed as a one-degree-of-freedom Hamiltonian system, the Cartesian coordinates x and y serving as the displacement and the associated momentum. For small values of β, equation (B1) can be rewritten as

$$H = [cR_2\Omega\psi^{ROT}]_{\beta=0}\sin(2\pi t/T + \delta) + \beta[2\pi R_0 R_1 \psi^{EXP}/T]_{\beta=0}\sin(2\pi t/T) + O(\beta^2). \tag{B 2}$$

Thus, in the absence of the cylinders' radial motion, the Hamiltonian H_0 can be defined as

$$H_0(x, y, t) = [cR_2\Omega\psi^{ROT}]_{\beta=0}\sin(2\pi t/T + \delta) \tag{B 3}$$

where the term in square brackets is time independent (the geometry of the system remains fixed if $\beta = 0$).

The system of differential equations associated with H_0 that describe the fluid particle motion is

$$\frac{\mathrm{d}x}{\mathrm{d}t} = \frac{\partial H_0}{\partial y} = \left[cR_2\Omega\frac{\partial\psi^{ROT}}{\partial y}\right]_{\beta=0}\sin(2\pi t/T + \delta), \tag{B 4a}$$

$$\frac{\mathrm{d}y}{\mathrm{d}t} = -\frac{\partial H_0}{\partial x} = -\left[cR_2\Omega\frac{\partial\psi^{ROT}}{\partial x}\right]_{\beta=0}\sin(2\pi t/T + \delta). \tag{B 4b}$$

Clearly, this system is integrable (simply 'divide' (B4b) by (B4a) to obtain that $\mathrm{d}y/\mathrm{d}x$ is time independent). Thus, the streamline map shown in figure 1(b) remains unchanged for all times and all trajectories are regular.

The perturbation induced by the radial motion of the cylinders is governed by the Hamiltonian

$$H' = \beta[2\pi R_0 R_1 \psi^{EXP}/T]_{\beta=0}\sin(2\pi t/T) \tag{B 5}$$

where H' vanishes as β diminishes to zero. Note that also here the expression in square brackets is time independent.

It is interesting to note that for cases in which $\delta = 0$ (the rhythmical expansion of the alveoli is in phase with the tidal flow) the Hamiltonian $H = H_0 + H'$ is still integrable. Only if the tidal flow and the flow induced by alveolus expansion are out of phase may one expect chaos. Thus, to apply the KAM theorem one should expand H_0 with respect to δ and consider the following separation of H:

$$\begin{aligned} H = {} & \{[cR_2\Omega\psi^{ROT}]_{\beta=0} + \beta[2\pi R_0 R_1\psi^{EXP}/T]_{\beta=0}\}\sin(2\pi t/T) \\ & + \delta[cR_2\Omega\psi^{ROT}]_{\beta=0}\cos(2\pi t/T) + O(\beta^2) + O(\delta^2). \end{aligned} \tag{B 6}$$

Here, the product of the expression in curly brackets with $\sin(2\pi t/T)$ represents the Hamiltonian associated with the integrable system while that shown by the second line is the Hamiltonian of the perturbed system. For δ sufficiently small, the KAM

theorem would apply since the latter vanishes as $\delta \to 0$ (for more conditions required by the KAM theorem, satisfied in our case, see Tabor 1989.)

Appendix C

Employing (3) it is easy to show that

$$\left.\begin{aligned} v_x = \frac{\mathrm{d}x}{\mathrm{d}t} &= \frac{c}{(\cosh\eta - \cos\xi)^2}\left(-\hat{c}\frac{\mathrm{d}\eta}{\mathrm{d}t} - \hat{s}\frac{\mathrm{d}\xi}{\mathrm{d}t}\right) + \frac{\sinh\eta}{\cosh\eta - \cos\xi}\frac{\mathrm{d}c}{\mathrm{d}t}, \\ v_y = \frac{\mathrm{d}y}{\mathrm{d}t} &= \frac{c}{(\cosh\eta - \cos\xi)^2}\left(\hat{c}\frac{\mathrm{d}\xi}{\mathrm{d}t} - \hat{s}\frac{\mathrm{d}\eta}{\mathrm{d}t}\right) + \frac{\sin\xi}{\cosh\eta - \cos\xi}\frac{\mathrm{d}c}{\mathrm{d}t}, \end{aligned}\right\} \tag{C 1}$$

where

$$\hat{c} = \cosh\eta\cos\xi - 1 \text{ and } \hat{s} = \sinh\eta\sin\xi$$

However, the Cartesian velocity components are given by

$$v_x = \frac{\partial\Psi}{\partial y} = (1/c)\left(\hat{c}\frac{\partial\Psi}{\partial\xi} - \hat{s}\frac{\partial\Psi}{\partial\eta}\right), \quad v_y = -\frac{\partial\Psi}{\partial x} = (1/c)\left(-\hat{c}\frac{\partial\Psi}{\partial\eta} - \hat{s}\frac{\partial\Psi}{\partial\xi}\right) \tag{C 2}$$

Substituting (B2) into (B1) and employing the identity $\hat{c}^2 + \hat{s}^2 = (\cosh\eta - \cos\xi)^2$ equations (24) are recovered.

REFERENCES

Aref, H. 1984 Stirring by chaotic advection. *J. Fluid Mech.* **143**, 1–21.

Aref, H. & Balachandar, S. 1986 Chaotic advection in a Stokes flow. *Phys. Fluids* **29**, 3515–3521.

Ballal, B. Y. & Rivlin, R. S. 1976 Flow of a Newtonian fluid between eccentric rotating cylinders: Inertial effects. *Arch. Rat. Mech. Anal.* **62**, 237–294.

Darquenne, C. & Pavia, M. 1996 Two- and -three dimensional simulations of aerosol transport and deposition in alveolar zone of human lung. *J. Appl. Physiol.* **80**, 2889–2898.

Darquenne, C. 2001 A realistic two dimensional model of aerosol transport and deposition in the alveolar zone of the human lung. *J. Aerosol Sci.* **32**, 1161–1174.

Federspiel, W. J. & Fredberg, J. J. 1988 Axial dispersion in respiratory bronchioles and alveolar ducts. *J. Appl. Physiol.* **64**, 2614–2621.

Fredberg, J. J. 2000. Frozen objects: small airways, big breaths, and asthma. *J Allergy Clin Immunol.* **106**, 615–624.

Gradshtyn, I. S. & Ryzhik, I. M. 1984 *Tables of Integrals, Series, and Products*, 5th edn. Academic.

Haber, S., Butler, J. P., Brenner, H., Emanuel, I. & Tsuda, A. 2000 Shear flow over a self similar expanding pulmonary alveolus during rhythmical breathing. *J. Fluid Mech.* **405**, 243–268.

Haber, H. & Tsuda, A. 2003 Gravitational deposition in a rhythmically expanding and contracting alveolus. *J. Appl. Physiol.* **95**, 657–671.

Happel, J. & Brenner, H. 1983 *Low Reynolds Number Hydrodynamics.* Kluwer.

Henry, F. S., Butler, J. P. & Tsuda, A. 2002 Kinematically irreversible flow and aerosol transport in the pulmonary acinus: a departure from classical dispersive transport. *J. Appl. Physiol.* **92**, 835–845.

Horner, M., Metcalfe, G., Wiggins, S. & Ottino, J. M. 2002 Transport enhancement mechanisms in open cavities. *J. Fluid Mech.* **452**, 199–229.

Hydon, P. E. 1994 Resonant advection by oscillatory flow in a curved pipe. *Physica* D **76**, 44–54.

Hydon, P. E. 1994 Resonant and chaotic advection in a curved pipe. *Caos, Solitons Fractals* **4**, 941–954.

Karl, A., Henry, F. S. & Tsuda, A. 2004 Low Reynolds number viscous flow in an alveolated duct. *Trans. ASME: J. Biomech. Engng* **126**, 13–19.

Lichtenberg, A. J. & Lieberman, M. A. 1992 *Regular and Chaotic Dynamics.* Springer.

Miki, H., Butler, J. P., Rogers, R. A., & Lehr, J. 1993 Geometric hysteresis in pulmonary surface to volume ratio during tidal breathing. *J. Appl. Physiol.* **75**, 1630–1636.

Ottino, J. M., Leong, C. W., Rising, H. & Swanson, P. D. 1988 Morphological structures produced by mixing in chaotic flows. *Nature* **333**, 419–425.

Ottino, J. M. 1989 *The Kinematics of Mixing: Stretching, Chaos, and Transport*. Cambridge University Press.

Pozrikidis, C. 1994 Shear flow over a plane wall with an axisymmetric cavity or a circular orifice of finite thickness. *Phys. Fluids* **6**, 68–79.

Solomon, T. H., Weeks, E. R. & Swinney, H. L. 1994 Chaotic advection in a two-dimensional flow: Levy flights and anomalous diffusion. *Physica* D **76**, 70–84.

Tabor, M. 1989 *Chaos and Integrability in Nonlinear Dynamics*. Wiley.

Tippe, A. & Tsuda, A. 2000 Recirculating flow in an expanding alveolar model: experimental evidence of flow-induced mixing of aerosols in the pulmonary acinus. *J. Aerosol Sci.* **31**, 979–986.

Tsuda, A., Butler, J. P. & Fredberg, J. J. 1994*a* Effects of alveolated duct structure on aerosol kinetics. I. diffusional deposition in the absence of gravity. *J. Appl. Physiol.* **76**, 2497–2509.

Tsuda, A., Butler, J. P. & Fredberg, J. J. 1994*b* Effects of alveolated duct structure on aerosol kinetics. II. Gravitational sedimentation and inertial impaction. *J. Appl. Physiol.* **76**, 2510–2516.

Tsuda, A., Federspiel, W. J., Grant, Jr, P. A. & Fredberg, J. J. 1991 Axial dispersion of inert species in alveolated channels. *Chem. Engng Sci.* **46**, 1419–1426.

Tsuda, A., Henry, F. S. & Butler, J. P. 1995 Chaotic mixing of alveolated duct flow in rhythmically expanding pulmonary acinus. *J. Appl. Physiol.* **79**, 1055–1063.

Tsuda, A., Rogers, R. A., Hydon, P. E. & Butler, J. P. 2002 Chaotic mixing deep in the lung. *Proc. Natl Acad. Sci. USA* **99**, 10173–10178.

Weibel, E. R. 1963 *Morphology of the lung*. Academic.

Weibel, E. R. 1986 Functional morphology of lung parenchyma. In: *Handbook of Physiology, The Respiratory System* (ed. A. P. Fishman), sect. 3, vol. III, chap. 8, pp. 89–111. American Physiology Society, Bethesda, MD.